




Article

Spatial and Temporal Distribution of PM_{2.5} Pollution over Northeastern Mexico: Application of MERRA-2 Reanalysis Datasets

Johana M. Carmona ¹, Pawan Gupta ^{2,3}, Diego F. Lozano-García ¹, Ana Y. Vanoye ¹,
Fabiola D. Yépez ⁴ and Alberto Mendoza ^{1,*}

¹ Tecnológico de Monterrey, Escuela de Ingeniería y Ciencias, Ave. Eugenio Garza Sada 2501, Monterrey 64849, Mexico; jcarmona.phd.mty@itesm.mx (J.M.C.); dflozano@tec.mx (D.F.L.-G.); avanoye@tec.mx (A.Y.V.)

² Science and Technology Institute, Universities Space Research Association (USRA), Huntsville, AL 35806, USA; pawan.gupta@nasa.gov

³ NASA Marshall Space Flight Center, Huntsville, AL 35805, USA

⁴ Facultad de Ingeniería Civil, Universidad Autónoma de Nuevo León, San Nicolás de los Garza 66455, Mexico; fabiola.yepezn@uanl.edu.mx

* Correspondence: mendoza.alberto@tec.mx; Tel.: +52-81-8358-2000 (ext. 5219)

Received: 12 May 2020; Accepted: 14 July 2020; Published: 16 July 2020



Abstract: Aerosol and meteorological remote sensing data could be used to assess the distribution of urban and regional fine particulate matter (PM_{2.5}), especially in locations where there are few or no ground-based observations, such as Latin America. The objective of this study is to evaluate the ability of Modern-Era Retrospective Analysis for Research and Application, version 2 (MERRA-2) aerosol components to represent PM_{2.5} ground concentrations and to develop and validate an ensemble neural network (ENN) model that uses MERRA-2 aerosol and meteorology products to estimate the monthly average of PM_{2.5} ground concentrations in the Monterrey Metropolitan Area (MMA), which is the main urban area in Northeastern Mexico (NEM). The project involves the application of the ENN model to a regional domain that includes not only the MMA but also other municipalities in NEM in the period from January 2010 to December 2014. Aerosol optical depth (AOD), temperature, relative humidity, dust PM_{2.5}, sea salt PM_{2.5}, black carbon (BC), organic carbon (OC), and sulfate (SO₄²⁻) reanalysis data were identified as factors that significantly influenced PM_{2.5} concentrations. The ENN estimated a PM_{2.5} monthly mean of 25.62 µg m⁻³ during the entire period. The results of the comparison between the ENN and ground measurements were as follows: correlation coefficient $R \sim 0.90$; root mean square error = 1.81 µg m⁻³; mean absolute error = 1.31 µg m⁻³. Overall, the PM_{2.5} levels were higher in winter and spring. The highest PM_{2.5} levels were located in the MMA, which is the major source of air pollution throughout this area. The estimated data indicated that PM_{2.5} was not distributed uniformly throughout the region but varied both spatially and temporally. These results led to the conclusion that the magnitude of air pollution varies among seasons and regions, and it is correlated with meteorological factors. The methodology developed in this study could be used to identify new monitoring sites and address information gaps.

Keywords: MERRA-2; PM_{2.5}; aerosol optical depth (AOD); air pollution; satellite data; neural networks

1. Introduction

Ambient particulate matter (PM) with aerodynamic diameter less than 2.5 µm (PM_{2.5}) is known to have adverse effects on visibility, ecosystems, and climate change [1]. High levels of airborne particles also present a significant health risk, and their effects on human health are well-documented in the

literature. For example, a $10 \mu\text{g m}^{-3}$ increase in ambient air $\text{PM}_{2.5}$ concentration has shown to have a significant increase in the risk of neurological disorders (i.e., stroke, dementia, Alzheimer's disease, and Parkinson's disease) [2], as well as respiratory, cardiovascular, and cerebrovascular [3] morbidity and mortality in all ages [4,5] of the exposed population.

Air pollution control policies, such as stricter emission standards, cleaner fuels, relocation of polluting industries, and rezoning efforts, have helped to improve air quality in many parts of the world [6], thus reducing the socioeconomic burden associated with this issue. The full understanding of the spatiotemporal variations in air pollution exposures that occur due to local emissions sources, such as urban transportation and finer-scale meteorology, could help in identifying at-risk and vulnerable populations, control relevant emissions contributing to exposure, and protect public health [7].

The effective management of air pollution is limited by sparse monitoring networks. $\text{PM}_{2.5}$ shows substantial spatiotemporal variability partly because of its short lifetime in the atmosphere. Therefore, surface measurements are fundamental in tracking the ground-level concentrations of $\text{PM}_{2.5}$, and protocols have been developed to ensure that these measurements provide a reliable description of the composition of the atmosphere within a certain spatial radius of the monitoring site. However, the monitoring of network coverage can be restricted by the high investment costs of running and maintaining surface monitoring sites [8]; for example, most monitoring sites in Latin America are located in the country's capital city and in a few major cities [9]. Low-cost portable monitors can be used to complement existing networks, and they are now being implemented in some municipalities around the world, including the Monterrey Metropolitan Area in Mexico [10], but limitations in accuracy, precision and sensitivity are faced when using this technology [11,12]. Hence, alternative approaches are required to describe large-scale spatial distributions of $\text{PM}_{2.5}$.

Combined satellite retrieval and model simulation are promising methods for studying regional $\text{PM}_{2.5}$ distribution, as these techniques have benefited from the rapid development of satellite missions in the last two decades. For example, the launch of the Moderate-Resolution Imaging Spectroradiometer (MODIS) and the Multiangle Imaging SpectroRadiometer (MISR) instrument on board NASA's Terra (1999) and Aqua (2002) satellites has provided global measurements of aerosol optical depth (AOD). AOD is a measure of light extinction by aerosols in the atmospheric column, which can be correlated with surface PM concentrations [13,14] with spatial resolutions of 3–10 km in the case of MODIS aerosol products [15], although the quality of correlation may vary greatly within regions.

Satellite-derived AOD has been integrated into models to improve their capability in the reproduction of aerosol spatial distribution [16], such as the Modern-Era Retrospective Analysis for Research and Application, version 2 (MERRA-2) model. MERRA-2 is the first multi-decadal reanalysis in which meteorological and aerosol observations are jointly assimilated into a global assimilation system [17]. It has the potential to provide improved estimates of AOD and $\text{PM}_{2.5}$ compared to the model alone, and it provides much greater coverage than surface observations [7]. The $\text{PM}_{2.5}$ speciation provided by MERRA-2 is an additional tool for use in the study of air pollution [18].

An increasing number of studies have combined pollutant ground measurements and MERRA-2 reanalysis data. Song et al. (2018) [7] evaluated the ability of MERRA-2 aerosol products to reproduce the diurnal and seasonal variabilities in AOD and $\text{PM}_{2.5}$ recorded by surface measurements in the North China Plain. Qin et al. (2019) [19] and Xu et al. (2020) [20] analyzed the temporal-spatial variation in black carbon (BC) and its effects in Beijing. MERRA-2 BC concentrations were compared with continuous ground BC measurements, which affirmed its reliability in demonstrating large-scale and long-term variations in ground BC concentrations. Sitnov et al. (2020) [21] studied large-scale BC pollution over Northern Eurasia during Siberian forest fires in the summer of 2016 using MERRA-2 reanalysis data. Moreover, Mukkavilli et al. (2019) [22] assessed the use of MERRA-2 AOD data against ground measurements in air quality forecasting over the Australian continent in the period from 2002–2012, concluding that high-resolution reanalysis datasets must be considered. In Mexico, García-Franco (2020) [23] employed MERRA-2 carbon monoxide (CO) emissions to examine air quality in the Mexico City Metropolitan Area (MCMA) during the fuel shortage in January 2019.

The combination of ground-level concentrations and satellite retrievals into a robust model is not a straightforward task, but machine learning techniques have proven to be a valuable tool in this task. The use of machine learning techniques, including artificial neural networks (ANNs), for air quality applications has been explored for some time [24], and its feasibility has been demonstrated [25]. A neural network uses artificial neurons, which are the smallest units in data processing [26]. The types of ANN include the back-propagation neural network (BPNN) [27,28], multilayer perceptron (MLP) [29,30], radial basis function (RBF) [31,32], and adopted neuro-fuzzy inference systems (ANFIS) [33–35]. While most of the available work is aimed at long-term forecasting of criteria pollutants using meteorological variables and source emissions as predictors [36], the use of satellite-derived aerosol optical depth (AOD) variables or reanalysis data for training and testing ANNs is also being investigated with favorable results [25]. Still, the majority of satellite applications have not been tested in developing countries, typically having higher PM_{2.5} levels and distinctive emission source profiles [36,37].

The objective of this study is to evaluate the ability of MERRA-2 aerosol products to represent seasonal variations in the PM_{2.5} ground concentrations in the Monterrey Metropolitan Area (MMA) and in Northeastern Mexico. The paper's scope includes the development and validation of a neural network model that uses MERRA-2 products to analyze the spatial-temporal distribution of PM_{2.5} concentrations over a wide domain that includes not only the MMA but also other municipalities in Northeastern Mexico. To the authors' best knowledge, this study constitutes one of the first applications of reanalysis data (i.e., MERRA-2 aerosol and meteorology products) combined with neural network model for the estimation of PM_{2.5} in a Latin American urban area. It is also the first attempt to use MERRA-2 data to estimate PM_{2.5} concentrations in the MMA and to analyze the spatial and temporal distributions of PM_{2.5} pollution over NEM.

2. Data and Methods

An overview of the methodology is shown in Figure 1. In general, first, meteorological and aerosol data from ground monitoring stations and MERRA-2 datasets were collected, and spatially and temporally arranged into a new grid. Then, an ENN was developed and validated. The ENN relates ground-based and MERRA-2 data to estimate PM_{2.5} within the Monterrey Metropolitan Area (MMA) for a period covering from January 2010 to December 2014. This stage allowed for the evaluation of the ability of MERRA-2 products to represent ground-based PM_{2.5} measurements and the identification of the predictor variables to be incorporated to the ENN. Ten trained and cross-validated NNs were employed to construct an ensemble NN for the estimation of PM_{2.5} monthly averages using the resulting dataset. Finally, a method that uses the neural networks developed in the first stage and the MERRA-2 reanalysis data was used to estimate PM_{2.5} in a gridded domain covering the NEM. Based on these data, monthly pollution maps were generated to analyze the spatial and temporal distributions of PM_{2.5} concentration fields. Statistical metrics—linear correlation coefficient *R*, Root Mean Squared Error (*RMSE*), and Mean Absolute Error (*MAE*)—were computed to evaluate model performance. Details are provided below.

2.1. Study Area

Located in Northeastern Mexico, the MMA covers 7,615 km² and is the third largest urban area in Mexico, with a population of 4.7 million people, distributed in 18 municipalities [38]. The MMA concentrates over 40% of the population in this region, and is the second largest industrial center in the country, having many facilities in several productive sectors (e.g., cement, glass, metallurgy, petrochemical, food processing, electric utilities, assembly, etc.) [39].

The average elevation of the urbanized area is around 550 m.a.s.l. although it is surrounded by mountains in three of the four cardinal directions with varying heights that reach 3,400 m.a.s.l., which alters the natural dispersion of airborne particles, thus limiting the air quality in this zone [40]. The distance from Monterrey to the nearest seashore is approximately 315 km. Specifically, this study

is based on data collected from the lower and upper bounds at 23° Lat, -101.25° Lon and 28° Lat, -98.125° Lon, respectively (Figure 2).

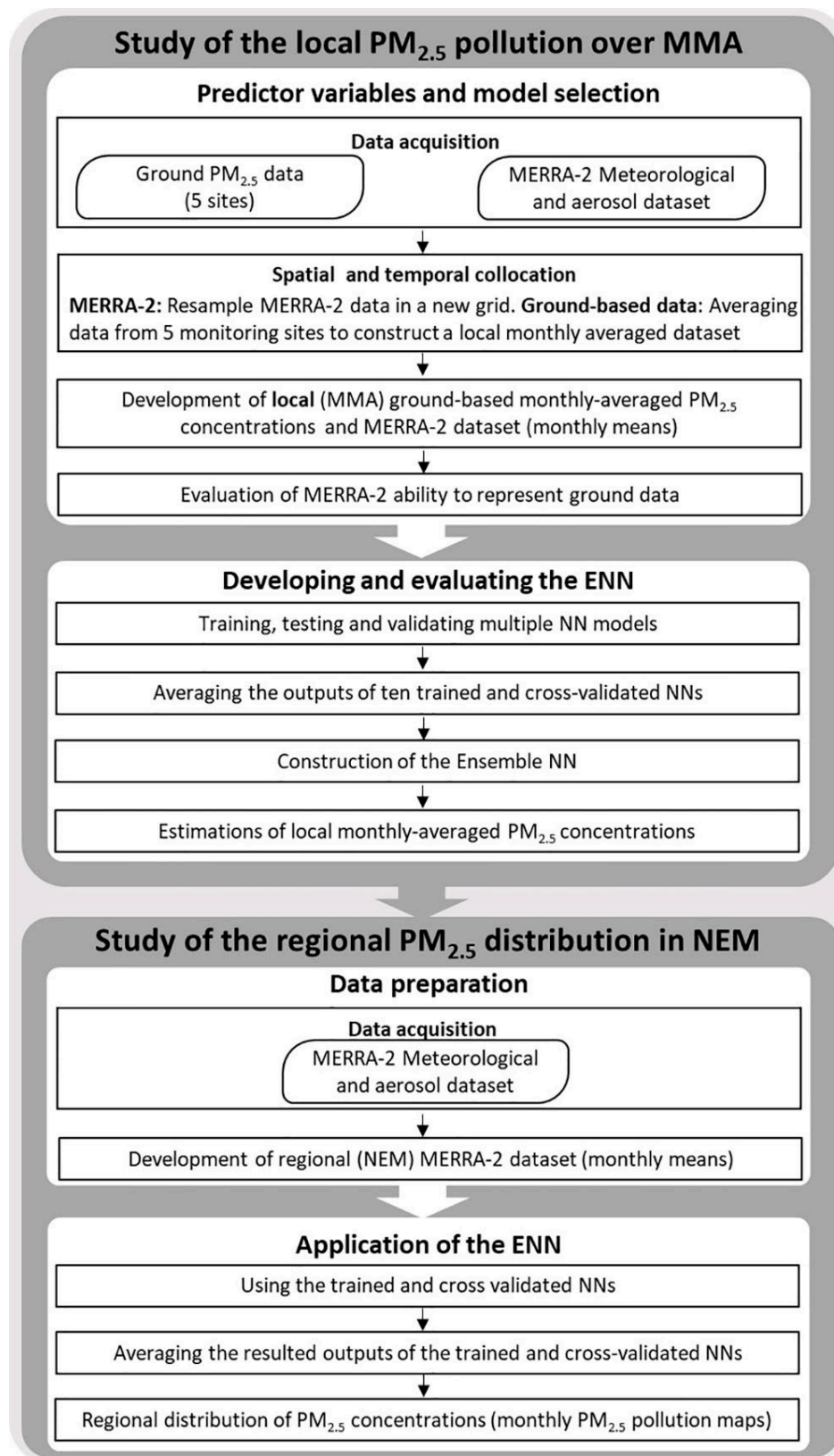


Figure 1. Methodological framework for analyzing the spatial-temporal distribution of $PM_{2.5}$.

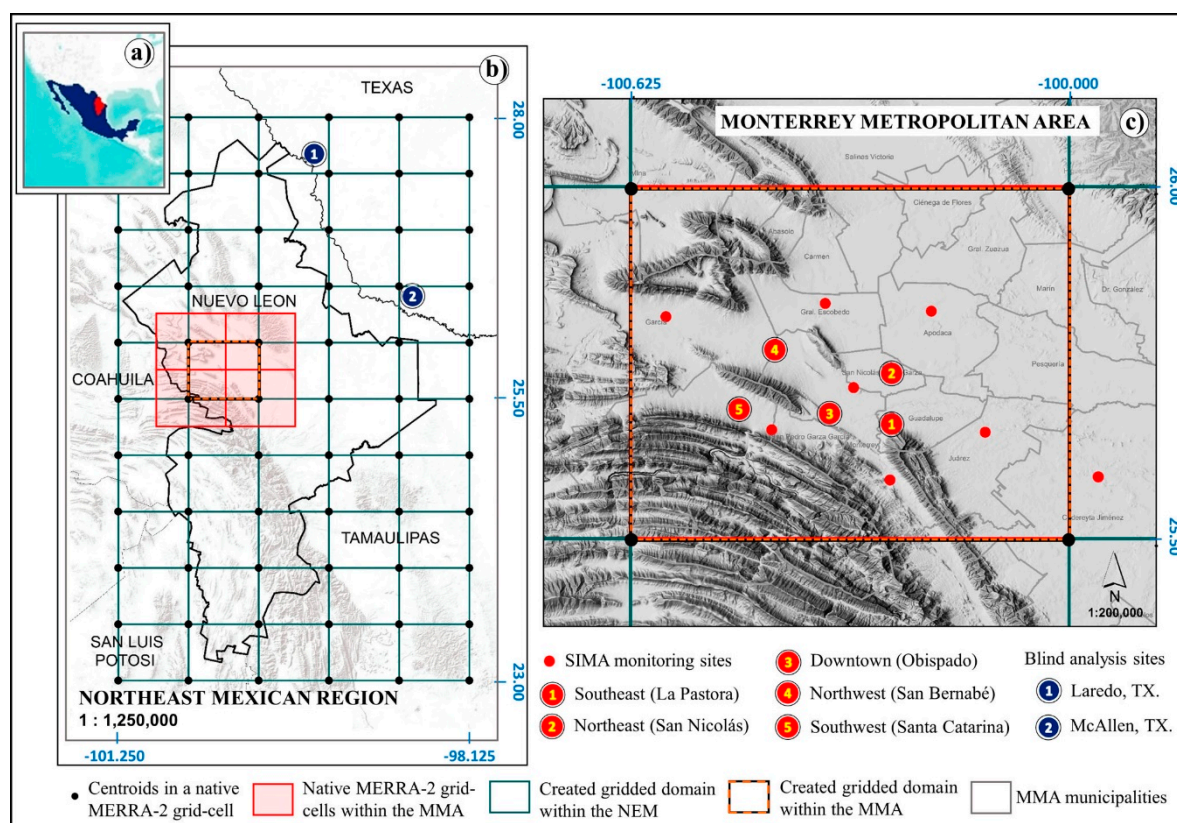


Figure 2. Study area location. (a) The MMA is located in the northeastern Mexican state of Nuevo Leon (shown in red). (b) Regional grid: vertexes correspond to the centroids of the native MERRA-2 grid. (c) Location of SIMA monitoring sites within the MMA.

The MMA frequently exceeds the national air quality standards for ozone (O_3), PM_{10} , and $PM_{2.5}$ [41]. According to the 2016 National Emission Inventory [42], 9,507 tons of $PM_{2.5}$ were emitted in the MMA in 2016, 13% of which came from point sources, 2% from non-road mobile sources, 77% from on-road mobile sources, and 7% from area sources. Previous studies on $PM_{2.5}$ source apportionment based on a chemical characterization and the use of organic molecular markers have also been conducted in the MMA [43,44]. These studies found that anthropogenic sources were a major contribution to secondary $PM_{2.5}$, where vehicle exhausts accounted for about 64% of the $PM_{2.5}$. Cooking operations and biomass burning were also found to be important sources [45]. Other sources identified in the MMA were industrial activities, garbage burning, biogenic emissions, and resuspended dust [46].

In contrast to other Mexican cities that have improved their air quality, the average concentrations of $PM_{2.5}$ in the MMA increased by $\sim 5 \mu g m^{-3}$ between 2013 and 2015 [47]. In routine monitoring network, annual averages of $PM_{2.5}$ were found in the range of 20–34 $\mu g m^{-3}$, which exceeded the corresponding national air quality standards of 12 $\mu g m^{-3}$ (annual average) [48]. Annual seasonal variations in the concentration of $PM_{2.5}$ were observed, in which the highest concentration was in winter, and the lowest concentration was in the first half of the fall season [49].

2.2. Ground-Based $PM_{2.5}$ and Meteorological Data

Since 1993, Nuevo León state authorities have operated a monitoring system for air quality. The Integrated Environmental Monitoring System (SIMA) currently consists of 13 monitoring stations located in the four cardinal directions and in the center of the city (Figure 2). Criteria pollutants (O_3 , SO_2 , NO_x , CO , $PM_{2.5}$ and PM_{10}) and meteorological variables (i.e., temperature, relative humidity, wind speed, wind direction, pressure, precipitation, and solar radiation) are monitored continuously, and the data are summarized in hourly averages. Calibration, maintenance procedures,

and quality assurance/quality control (QA/QC) follow the protocols established in the Mexican standards NOM-035-SEMARNAT-1993 [50] and NOM-156- SEMARNAT-2012 [51].

In this study, from January 2010 to December 2014, hourly $PM_{2.5}$ concentrations were retrieved from the SIMA network at five urban air-monitoring sites (Southeast, Northeast, Downtown, Northwest, and Southwest). These sites were selected because they provided the long-term data required for this research. Also, they are the only sites that provide continuous and valid $PM_{2.5}$ records during the study period. The $PM_{2.5}$ instruments were based on the beta-ray attenuation method (BAM) and continuous weighing with microbalance, which provided automatic, continuous measurements and concentration recording.

2.3. $PM_{2.5}$ and Meteorological Data from MERRA-2

Reanalysis combines model fields with observations distributed irregularly in space and time in a spatially complete gridded meteorological dataset based on an unchanging model [52]. Reanalysis products are obtained using a fixed data assimilation scheme and a global climate model that ingest all available observations every 6–12 h. The MERRA-2 is based mainly on the Goddard Earth Observing System Model, Version 5 (GEOS-5), which is a weather and climate capable model provided with atmospheric circulation and composition as well as oceanic and land components [17]. MERRA-2 is not only a meteorological reanalysis but also includes the assimilation of aerosol observations based on a version of the GEOS-5 model that is radiatively coupled to the Goddard chemistry, aerosol, radiation, and transport (GOCART) aerosol module. It includes the assimilation of bias-corrected AOD from both MODIS sensors and the Advanced Very High-Resolution Radiometer instruments, non-bias-corrected AOD from the Multiangle Imaging SpectroRadiometer (MISR) over bright surfaces, and AOD from the Aerosol Robotic Network (AERONET) [17,18,53].

MERRA-2 integrates observational data from earth observing satellites (EOS) and the GEOS-5 model to simulate the hydrological cycle of Earth [52] since the beginning of the satellite era [54]. The MERRA-2 system has many of the same basic features as the MERRA system, which were described by Rienecker et al. (2011) [52], but it includes several important updates to its physical parameterizations (e.g., the use of a cubed-gridded sphere, increased re-evaporation of frozen precipitation and cloud condensate, changes to the background gravity wave drag, and an improved relationship between ocean surface roughness and ocean surface stress) and analysis algorithms (e.g., the use of normalized pseudo relative humidity and updated background error statistics). The updates included numerous additional satellite observations both before and after the introduction of NOAA-18 in 2005 by the National Oceanic and Atmospheric Administration (NOAA), the use of version 2.1.3 of the Community Radiative Transfer Model (CRTM) of the assimilation of all satellite radiances, the bias correction of aircraft temperature observations, mass conservation and water balance, observation-corrected precipitation forcing, sea surface temperature (SST), and sea-ice concentration (SIC) boundary conditions based on high-resolution daily products [55].

In this study, air temperature, relative humidity, eastward wind component, and northward wind component were extracted from M2IMNPASM three-dimensional, monthly time-averaged, assimilated meteorological fields (instM_3d_asm_Np) at 850 hPa [56]. The surface wind speed was extracted from M2TMNXFLX two-dimensional, monthly time-averaged, surface flux diagnostics files (tavgM_2d_flux_Nx) [57]. The aerosol components were extracted from M2TMNXAER two-dimensional, monthly time-averaged, aerosol diagnostics files (tavgM_2d_aer_Nx) [58]. All scientific datasets (SDS) used in this research had a spatial resolution of $0.5^\circ \times 0.625^\circ$, as presented in Table 1.

Table 1. Meteorological and aerosol SDS from MERRA-2.

Type	Name	Long Name	Units
Meteorology	T	“air_temperature”	°C
	RH	“relative_humidity_after_moist”	%
	U	“eastward_wind”	m s ⁻¹
	V	“northward_wind”	m s ⁻¹
	SPEED	“Surface_wind_speed”	m s ⁻¹
Aerosol	BCSMASS	“Black_Carbon_Surface_Mass_Concentration”	µg m ⁻³
	DUSMASS25	“Dust_Surface_Mass_Concentration_PM_2.5”	µg m ⁻³
	OCSMASS	“Organic_Carbon_Surface_Mass_Concentration_ENSEMBLE”	µg m ⁻³
	SO4MASS	“SO4_Surface_Mass_Concentration_ENSEMBLE”	µg m ⁻³
	SSSMASS25	“Sea_Salt_Surface_Mass_Concentration_PM_2.5”	µg m ⁻³
	TOTEXTTAU	“Total_Aerosol_Extinction_AOT_[550_nm]”	unitless

2.4. Spatial and Temporal Collocation

MERRA-2 and ground-based PM_{2.5} data were georeferenced to geographic latitude/longitude (WGS84) coordinates. Both datasets were collocated in space and time as follows: Temporal collocation was performed by monthly averaging the ground-based observations per monitoring site. Daily averages per site (including daily averaged PM_{2.5} concentrations and meteorological data) were calculated according to Mexican standard NOM-025-SSA1-2014 [59], which requires a threshold of 75% data capture (i.e., 18 hourly records) in order to consider that data are valid and representative. Missing values were excluded from the analysis. When daily averages were available in at least four sites, a local daily averaged dataset (PM_{2.5} and meteorological data) was estimated. These local-daily averages were then averaged in a monthly basis to obtain a local monthly averaged dataset.

For spatial collocation, a new local grid covering the MMA was created by using the centroids of the native MERRA-2 grid as vertexes (Figure 2), which increased data representation over the MMA. A unique value for each variable in each grid cell was calculated by averaging data values at each cell centroids of the native MERRA-2 grid. Then, the local ground-based monthly averages were assigned to the grid cell contained within the lower and upper bounds at 25.5° Lat, −100° Lon and 26° Lat, −100.125° Lon, respectively. For the regional application, a domain contained within the lower and upper bounds at 23° Lat, −101.25° Lon and 28° Lat, −98.125° Lon, respectively, with grid cells at 0.5° × 0.625° latitude by longitude spatial resolution, the same as the native MERRA-2 resolution, was defined.

2.5. Evaluation of MERRA-2’s Ability to Represent Ground Data and Model Selection

AOD was found to have a strong positive relationship with PM_{2.5} concentrations observed on the surface [60,61], but there is also evidence that the use of AOD as the only predictor of PM_{2.5} is subject to large uncertainties [62]. Several variables, such as temperature, relative humidity, wind speed, wind direction, aerosol type, and height of the boundary layer (PBL), are the most commonly used as model covariates of AOD in estimating PM_{2.5} [60]. In this study, MERRA-2 AOD data were compared to ground-based PM_{2.5} measurements to determine its suitability as a proxy for PM_{2.5} in the MMA. The ability of MERRA-2 products to represent meteorological variables that are routinely measured in the MMA was evaluated, and MERRA-2 PM_{2.5} components were included to represent the aerosol type. Nitrates, which can be important components of the total PM_{2.5} mass, are not reported by MERRA-2 aerosol products. However, because of AOD assimilation, MERRA-2 total AOD is not affected by the lack of nitrates.

Local monthly averaged PM_{2.5} concentrations were compared to MERRA-2 total AOD using simple linear regression. Also, seasonal variations of PM_{2.5} concentrations were analyzed using time series. One-way analysis of variance (ANOVA) was used to test differences for temperature and relative humidity between MERRA-2 meteorological SDSs and local monthly averaged meteorology; simple linear regressions were performed to test correlation, too. Wind-roses analysis was performed to evaluate the models’ ability to replicate the predominant wind pattern in the MMA. Because

PM_{2.5} speciation measurements are not available on a routine and continuous basis in the MMA, MERRA-2 PM_{2.5} components were compared to previous PM_{2.5} speciation studies carried out in the area during specific monitoring campaigns. The variables with no statistical differences in the ANOVA test, with a significant correlation in the linear regression, or with similar temporal or seasonal behavior with respect to ground-based data were retained as predictors. In total, eight predictor variables were selected and PM_{2.5} concentration was estimated as a function of AOD, temperature (T), relative humidity (RH), dust PM_{2.5} (Dust), sea salt PM_{2.5} (SS), black carbon (BC), organic carbon (OC), and sulfate (SO₄²⁻) concentrations (Equation (1)).

$$PM_{2.5} = f(AOD, T, RH, Dust_{2.5}, SS_{2.5}, BC, OC, SO_4^{2-}) \quad (1)$$

2.6. Model Development

Several thousand multiple back-propagation MLP type ANN models were developed, trained, and validated using identical topology and neuron functions. Figure 3 depicts the ANN structure applied in this study for every individual NN, in which eight input factors were used, and one hidden layer led to one outcome. A sigmoid function was employed as the transfer function in the hidden layer, and the Levenberg-Marquardt (LM) algorithm [63] was employed in the training. Independent validation to evaluate the predictive performance of the trained NN was carried out using cross-validation [64] along the hold-out method [65]. Hold-out validation is the simplest form of cross-validation. Contrary to other methods, the split procedure is performed by separating the entire dataset, only once, into two independent groups, one for model development/calibration (training dataset) and the other for validation [66]. Then, the ensemble modeling approach was applied as a hybrid system to reduce the variance in predictions and to reduce the generalization error [67] produced by the hold-out method [65].

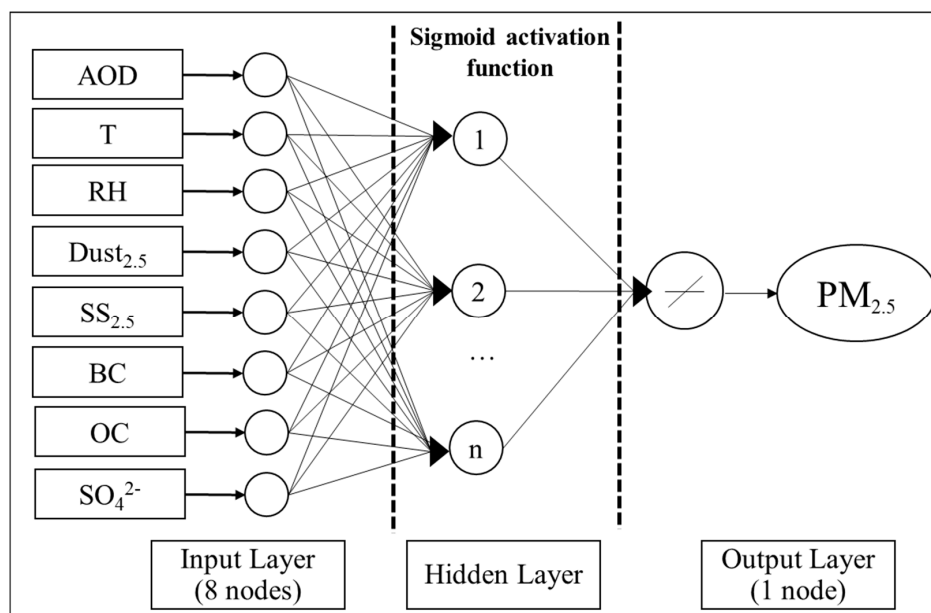


Figure 3. A schematic of the NN model used in this study to estimate PM_{2.5}.

The NNs were developed using a database containing local monthly averaged PM_{2.5} concentrations and all MERRA-2 predictor variables included in Equation (1) for a period of 58 months, which corresponded to SIMA's data availability. The entire database was randomly divided into training and validation datasets: 70% of data was used to train the neural networks, while the remaining set (30% of data) was arranged to test the models' performance. The PM_{2.5} predictions (outputs) from the best ten trained and cross-validated NNs were averaged to build an ensemble NN to estimate the

local monthly averaged $PM_{2.5}$ ground concentrations over the MMA. R , $RMSE$ and MAE were used to evaluate the ENN performance, these metrics were computed for training and validation datasets in each NN, allowing consistent comparisons among them. The NNs with the best performance (highest R , and lowest $RMSE$ and MAE) in the validation subset were selected to build an ENN in which the individual predictions of the constituent NNs were combined using a simple averaging technique.

To avoid overfitting, an NN architecture was designed using the “simpler-structure principle” [68]. The early stopping method was then applied as the regularization technique [69]. According to the “simpler-structure principle,” the optimal structure of a NN should be fairly simple, having several nodes in one hidden layer. In this study, the training was begun with the simplest structure (only one node in the hidden layer) and the local optimum was sought on the validation error curve. The procedure was performed again using a new node, and the resulting value was compared to the previous minimum value. This process was repeated until a structure having fewer nodes in the hidden layer was obtained [70]. The stopping criteria were determined by a predefined threshold number of training iterations, the cross-validation approach [64], and the reduction of root mean squared error ($RMSE$) in a validation data set [71].

Once the ENN were validated over the MMA, the NN models were used to estimate the $PM_{2.5}$ over the NEM. The regional distribution of $PM_{2.5}$ was estimated using only MERRA-2 data as input into the NN. Monthly averaged $PM_{2.5}$ maps were generated for the regional gridded domain.

3. Results

3.1. MERRA-2 and Ground-Based Data: Comparisons

In this study, a simple linear correlation between the local monthly averaged $PM_{2.5}$ concentrations and AOD data over the MMA was not statistically significant (p -value < 0.01). However, the $PM_{2.5}$ ground-based concentrations exhibited a marked seasonal pattern throughout the entire study period (Figure 4). Maximum monthly concentrations were in the range of 30–35 $\mu\text{g m}^{-3}$, except May 2011 when $PM_{2.5}$ registered a maximum value of 38 $\mu\text{g m}^{-3}$. AOD varied in the range of 0.05–0.25, which is typical of very clean to moderately polluted atmospheres. However, it also registered a maximum value of 0.36 in May 2011, which is very close to 0.4 and characteristic of high pollution conditions [72].

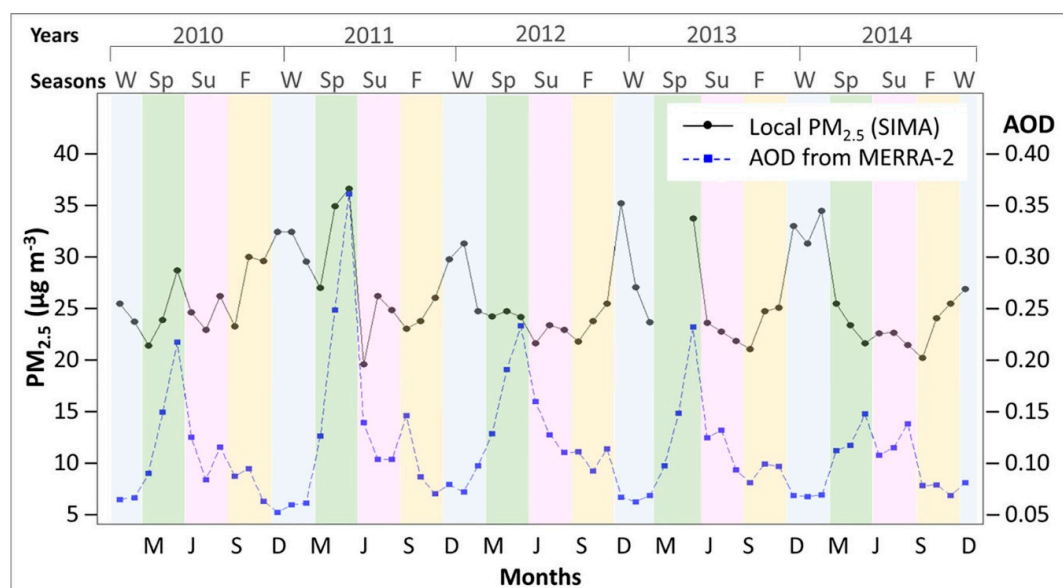


Figure 4. Comparison of temporal behavior of monthly AOD means obtained from MERRA-2 and the local monthly average $PM_{2.5}$ concentrations over the MMA (derived from SIMA data) from January 2010 to December 2014. Seasons: W: Winter, Sp: Spring, Su: Summer, F: Fall. Months: M: March; J: June, S: September, D: December.

The AOD and ground-based $PM_{2.5}$ concentrations showed distinct seasonal differences: the ground $PM_{2.5}$ values were higher in winter ($\geq 30 \mu\text{g m}^{-3}$), while AOD was the highest in spring (≥ 0.20). These differences were due to the complex relationship between $PM_{2.5}$ and AOD, which is influenced by aerosol type, chemical composition particle size, vertical concentration profile, and so on [73–78]. Smaller differences between $PM_{2.5}$ and AOD occurred during the springtime. In spring, the lower relative humidity—compared to other seasons and relatively strong atmospheric dispersion—may have enhanced the correlation between AOD and $PM_{2.5}$ [79]. Similar meteorological conditions in the MMA were reported by Carrillo Torres et al. (2017) [80] and Mancilla et al. (2015) [43].

The results of the ANOVAs revealed statistically significant differences (p -value < 0.01) when comparing the temperature and relative humidity SDS to monthly averaged ground-based data. The simple linear regression showed the ability of meteorological SDSs to represent the monthly average ground-based temperature ($R^2 = 0.92$) and relative humidity ($R^2 = 0.60$) data over the MMA (Figure 5a,b). The wind components from MERRA-2 were not able to represent the predominant wind pattern (i.e., east-to-west direction) and the wind speeds observed in the MMA from 2010–2014, as shown in Figure 5c,d. Thus, the wind components from MERRA-2 were not incorporated into the NN model.

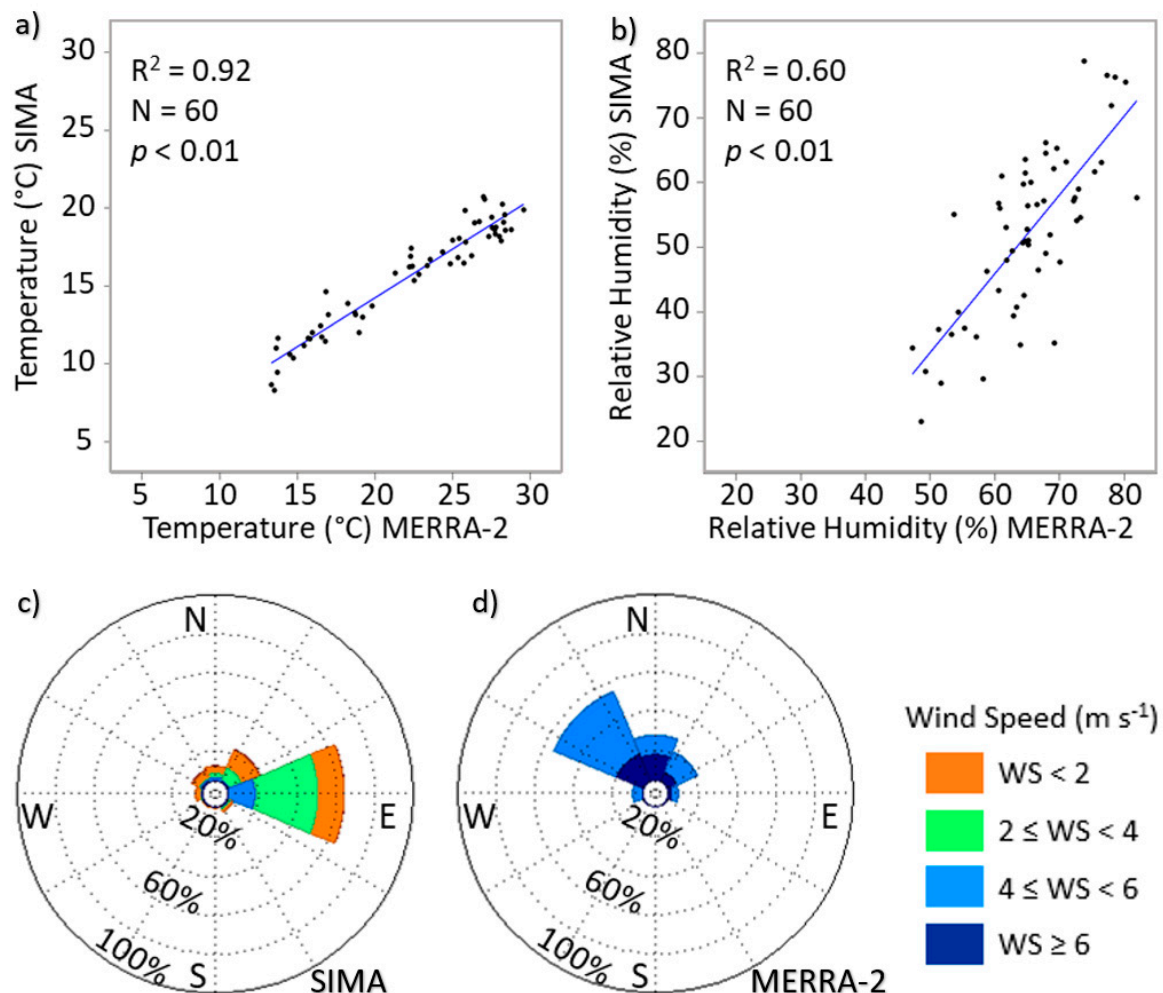


Figure 5. Comparison between the MERRA-2 meteorological data and monthly average ground-based data in the MMA from January 2010 to December 2014. (a) monthly temperature mean correlations; (b) monthly relative humidity mean correlations; (c) wind rose using wind components from SIMA; (d) wind rose using wind components from MERRA-2.

According to the data extracted from MERRA-2, during most of the study period, the main components of $PM_{2.5}$ were sulfates (33%) and OC (29%) (Figure 6), which were similar to the findings of Martínez et al. (2012) [44], Blanco-Jiménez et al. (2015) [49], and Mancilla et al. (2019) [48]. Mancilla et al. (2019) [48] revealed that anthropogenic sources were typically associated with high contributions of SO_4^{2-} , OM, and BC. Secondary inorganic aerosols in the form of ammonium nitrates that were not reported by MERRA-2 were found to be important compounds in the MMA [81].

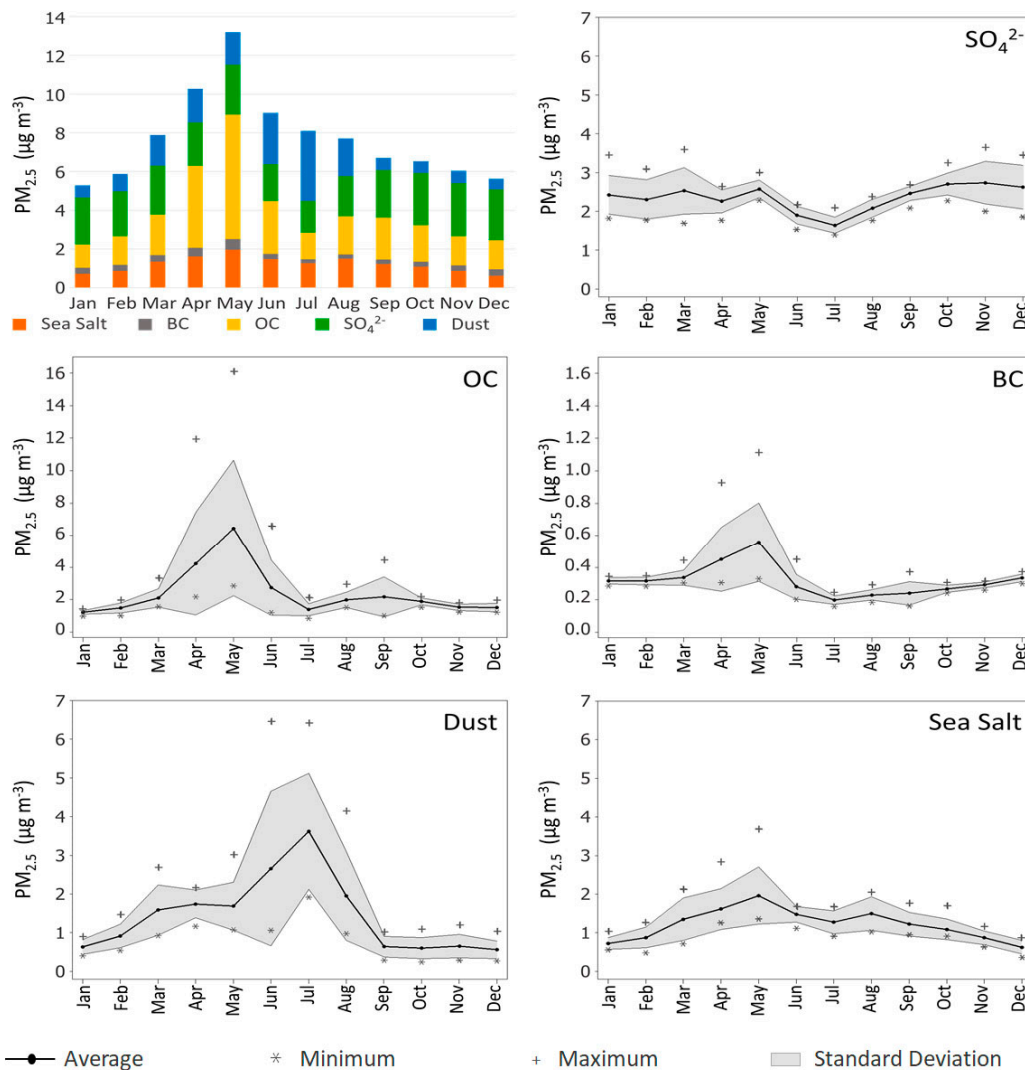


Figure 6. Annual $PM_{2.5}$ profile from MERRA-2 over the MMA from January 2010 to December 2014. Upper left panel: annual profiles of all $PM_{2.5}$ components. Upper right panel and lower panels: annual $PM_{2.5}$ profile by component.

The SO_4^{2-} component showed the lowest temporal variability (standard deviation = $\pm 0.3 \mu g m^{-3}$ and coefficient of variation = 14%). SO_4^{2-} monthly means remained between $2 \mu g m^{-3}$ and $3 \mu g m^{-3}$ during the study period, except the summer months when the averages decreased from 7–10% (or $<2 \mu g m^{-3}$). These results contradicted the seasonal SO_4^{2-} behavior reported by González et al. (2018) [82], who concluded that in the MMA, as in other parts of the world, the lower conversion of SO_2 to SO_4^{2-} ions occurs in winter. González et al. (2018) [82] suggested that lower solar radiation and lower relative humidity characteristics of winter might lead to the lower photochemical oxidation of SO_2 . This disparity might also be explained by the prevailing meteorological conditions in summer when stronger wind flows from the coastal zone ($SE \geq 80\%$ and $WS \geq 10 km h^{-1}$) influence the atmospheric stability-mixing processes, and hence the concentration of air pollutants [83]. Based on the results of

the present study, the further understanding of these dilution effects or “urban fluid mechanics” [84] is recommended, which would clarify the effects of SO₂ oxidation rates on the residence time of SO₂ and help determine whether dry deposition was relevant in the chemical conversion to SO₄²⁻.

The highest MERRA-2 monthly average OC (>4 µg m⁻³) and BC (>0.4 µg m⁻³) concentration occurred from April–June, which was in accordance with findings by Peralta et al. (2019) [85]. During these months, photochemical activity and transport were predominant over the MMA, promoting the aging of primary emissions into secondary organic aerosol (SOA), which constituted between 59 and 87% of total OC and 32–45% of PM_{2.5} in the area [43]. Moreover, despite the dissimilarity in spatial resolution, the MERRA-2 BC concentrations were consistently 7.5 times lower than the ground-based BC concentrations from January to April and from August to November. The exception was in the summer months when the MERRA-2 BC concentrations were approximately 13 times lower than those reported by Peralta et al. (2019) [85].

The highest monthly average dust concentrations (1.94–3.62 µg m⁻³) occurred in summer, while the highest monthly sea salt (SS) means were observed in spring (1.96 µg m⁻³), followed by summer (1.96 µg m⁻³). Because the MMA is not a local source of SS, it and dust are wind-dependent components. Therefore, the SS concentrations over the MMA can be attributed mainly to long-range transport. During spring and summer, wind speeds reach maximum values above 10 km h⁻¹, blowing primarily from the east (E) in the Gulf of Mexico region to the west (W) [86].

Table 2 shows the results of the comparison of the PM_{2.5} component concentrations (in µg m⁻³) obtained from MERRA-2 with those reported in previous ground-based studies conducted in the MMA. It must be noted that although the timeline was the same, the temporal and spatial resolutions differed among the data sets. Typically, local monitoring campaigns are conducted to study air quality in specific locations and periods. Here, the components determined in local studies are reported as daily mean concentrations. Conversely, the MERRA-2 aerosol data used in this study were extracted and monthly averaged to represent the air quality over a grid box (Figure 2).

Table 2. Comparison of PM_{2.5} concentrations (µg m⁻³) in components reported by MERRA-2 (M-2) with those reported in other MMA studies.

Period Component	Nov–Dec 2007			Dec 2014–Mar 2015			Jun–Jul 2015		
	(1)	M-2	Ratio	(2)	M-2	Ratio	(3)	M-2	Ratio
BC	2.74	0.27	10.15	2.07	0.33	6.27	0.35	0.20	1.75
OC	13.6	1.18	11.53	4.92	1.30	3.78	1.89	1.33	1.42
Dust	4.67	0.55	8.49	7.67	0.52	14.75	0.53	6.43	0.08
SO ₄ ²⁻	6.4	2.92	2.19	6.79	3.23	2.10	3.39	1.47	2.31
Sea Salt	1.4	0.94	1.49	0.59	0.60	0.98	0.09	1.67	0.05
OC/BC	4.96	4.37	1.13	2.38	3.94	0.60	5.40	6.65	0.80

(1) Martínez et al. (2012) [44], (2) Blanco-Jiménez et al. (2015) [49], (3) Mancilla et al. (2019) [48].

Despite the differences in temporal and spatial resolution, some similarities were observed. SO₄²⁻ derived by MERRA-2 was consistently ~2 times lower than the SO₄²⁻ reported by local studies, which might suggest not only the contribution of local sources, but also that SO₄²⁻ could be spatially and temporally homogeneous over the MMA. Additionally, the OC/BC ratios of PM_{2.5} derived by MERRA-2 ranged from 3.94 to 6.65, whereas those reported by previous ground-based local studies ranged from 2.38 to 5.40, indicating that MERRA-2 aerosol products are able to produce temporal OC/BC variations similar to those observed in the MMA; that is, seasonal variations in OC/BC could be captured by MERRA-2. OC/BC ratios exceeding 2 may reflect the combined contributions of charcoal combustion, motor-vehicle exhausts, and biomass burning sources, which are common in SOA formation [87], although they also indicate contributions from other primary sources with high OC/BC emission ratios [88].

3.2. Model Performance

The model performance of the ENN is presented in Figure 7. The ENN estimated a monthly $PM_{2.5}$ mean of $25.62 \mu g m^{-3}$ with the following metrics: $R \sim 0.90$, $RMSE = 1.81 \mu g m^{-3}$ and $MAE = 1.31 \mu g m^{-3}$. The measure of bias showed seasonal dependence, which was reported by other studies that used MERRA-2 aerosol data in other regions of the world (Table 3).

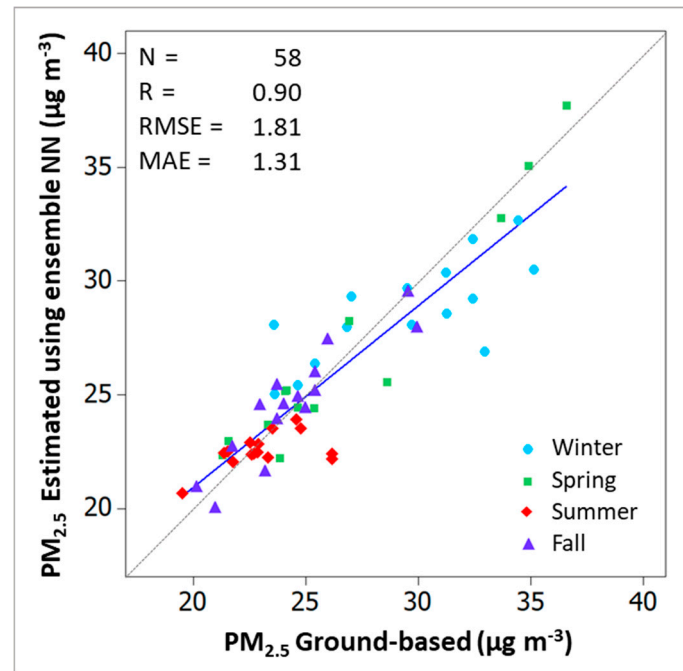


Figure 7. Statistical performance obtained using the ensemble NN to estimate monthly $PM_{2.5}$ means over the MMA from January 2010–December 2014.

Table 3. Previous studies that used MERRA-2 aerosol data to estimate $PM_{2.5}$ concentrations and compared them with monthly averaged ground-based concentrations or analyzed seasonal variations.

Study	Region and Period *	Model or Method *	Seasonal Performance
(1)	Pearl River Delta, Hong Kong, China. (2010–2013)	$PM_{2.5(Est)} = extinction / G(RH)$ where $G = \frac{A}{(100-RH)^\lambda}$ <i>A</i> and λ are determined by non-linear least square fitting.	Worst performance in spring, best in winter
(2)	China Country (2013–2014)	Geographically weighted regression (GWR), Back-propagation NN (BPNN), Generalized regression neural network (GRNN) model. MERRA-2 Variables: PBL, T, RH, wind speed, surface pressure	Best performance in summer; worst in winter
(3)	North China Plain, China (2014–2017)	$PM_{2.5} = 1.375 \times SO_4 + 1.6 \times OC + BC + Dust_{2.5} + SS_{2.5}$	Best performance in summer; worst in winter
(4)	Delhi, India (2016–2017)	Chemical Transport Model (CTM) MERRA-2 Variables: AOD, PBL, T, U and V wind components, $PM_{2.5}$ components	Best performance in spring; worst in winter and fall
(5)	Yangtze River Basin, China (2015–2016)	$PM_{2.5} = 1.375 \times SO_4 + 1.6 \times OC + BC + Dust_{2.5} + SS_{2.5}$	Best performance in summer, worst in winter
(6)	This study MMA, Mexico (2010–2014)	ENN $PM_{2.5} = f(AOD, T, RH, Dust_{2.5}, SS_{2.5}, BC, OC, SO_4^{2-})$	Best performance in spring, worst in winter

(1) Su et al. (2017) [89], (2) Li et al. (2017) [74], (3) Song et al. (2018) [7], (4) Alvarado et al. (2019) [90], (5) He et al. (2019) [91]. * To be compared in this study.

Ten trained and cross-validated NNs were used to construct the ensemble NN to calculate the monthly $PM_{2.5}$. Figure 8 shows the statistical performance (model fitting) of each NN. In the training fittings, the R values ranged between 0.85 and 0.89, whereas in the cross-validation, the R values ranged between 0.80 and 0.88. The differences between the R values of the training fittings and the R values of cross-validation ranged between -0.02 and 0.05 . The differences in the $RMSE$ ranged from

-0.60 to $0.16 \mu\text{g m}^{-3}$, and the differences in the MAE ranged from -0.39 to $0.13 \mu\text{g m}^{-3}$. These results suggested that the model was not over-fitted.

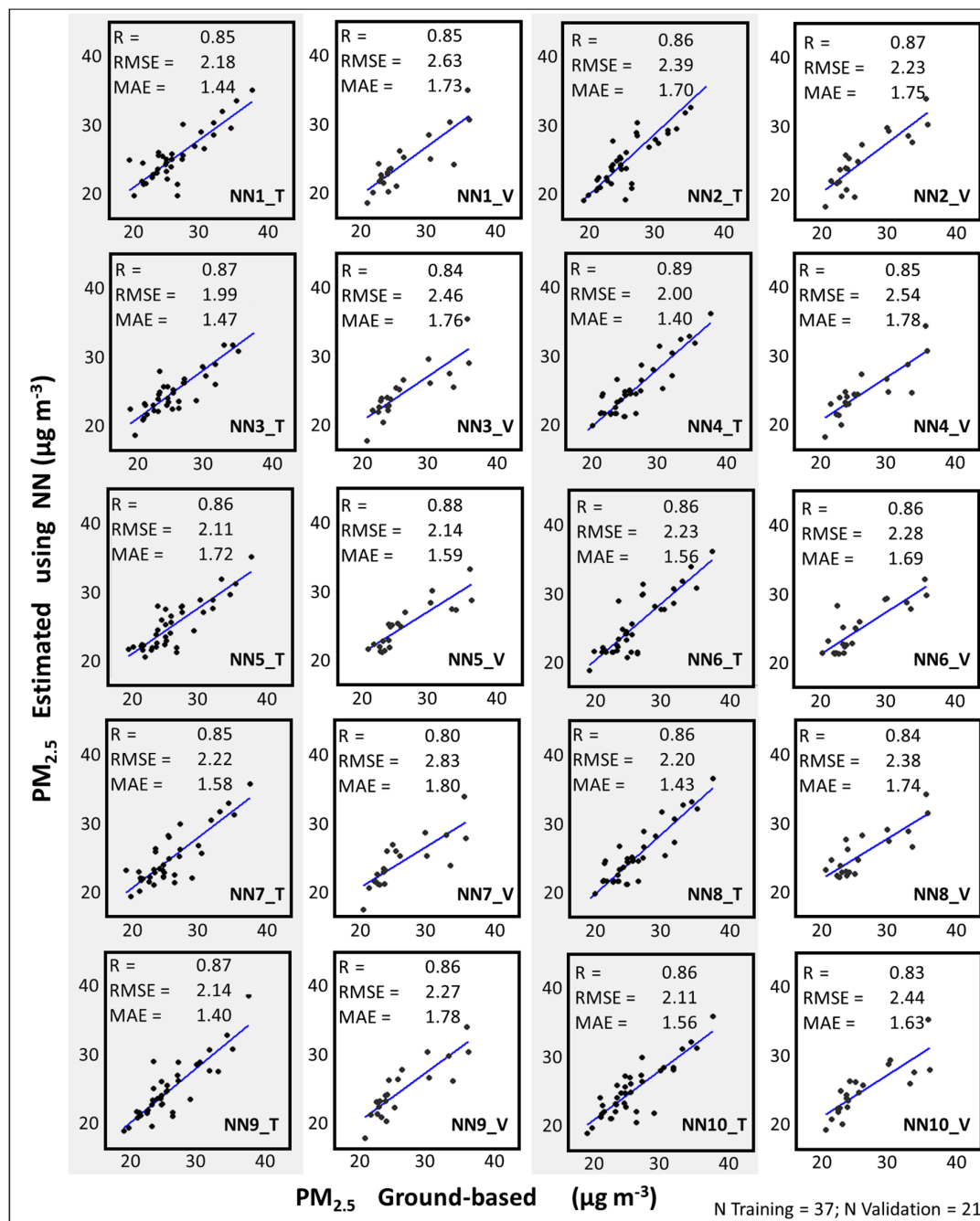


Figure 8. Statistical performance obtained from each NN used to construct the ensemble NN to estimate monthly $\text{PM}_{2.5}$ means over the MMA from January 2010–December 2014. Training (T) and validation (V) dataset.

3.3. Regional $\text{PM}_{2.5}$ Distribution

Monthly averaged $\text{PM}_{2.5}$ maps of the entire domain were generated to analyze the regional distribution of $\text{PM}_{2.5}$ (Figure 9). The heterogeneity of $\text{PM}_{2.5}$ concentrations in both space and time was observed. Overall, the $\text{PM}_{2.5}$ distributions on the annual and seasonal time-scales exhibited a consistent spatial pattern, and the highest $\text{PM}_{2.5}$ levels were located in the MMA, which was the main source of air pollution within the domain. These results indicated that $\text{PM}_{2.5}$ was not evenly

distributed around the MMA, perhaps because the mixed mountainous-and-valley topography acts as a physical barrier to natural wind circulation and complicates the dispersion of local emissions [82]. However, further research is needed to understand the relationship between air pollutants and urban morphology in the MMA.

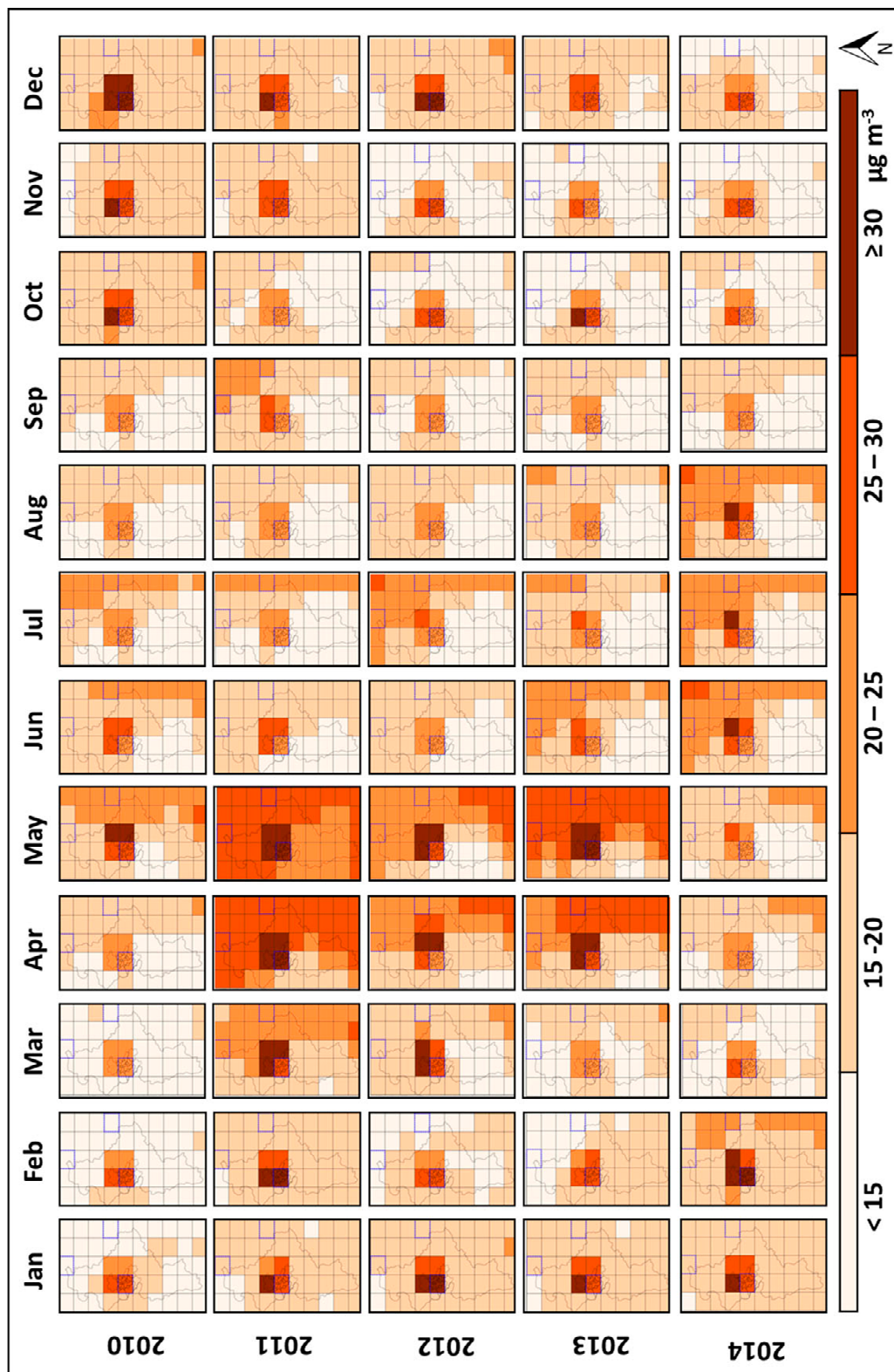


Figure 9. Regional distribution of monthly PM_{2.5} means in NEM.

The regional distribution of $PM_{2.5}$ also revealed seasonal variations. It was observed that in general, $PM_{2.5}$ levels were higher in winter and spring. Moreover, the month of May usually shows the largest concentrations (particularly the month of May 2011 and the month of May 2013) in the entire region, mainly caused by $PM_{2.5}$ emissions from biomass burning. In winter, concentrations increase due to the rise in emissions from burning fossil fuels, whether for heating [92], transportation, or cooking. However, meteorological conditions, especially those related to high pressure systems, thermal inversions, and low precipitation, also play an important role by inhibiting the dispersion and removal of pollutants [93]. Overall, the concentrations decrease from spring to summer and then increase from fall to winter. It could be concluded that regional air quality is worse in winter and slightly better in summer.

4. Discussion

Comparison of monthly $PM_{2.5}$ means ($\mu\text{g m}^{-3}$) estimated by the ENN developed in this study with the monthly $PM_{2.5}$ means from MERRA-2 derived data and monthly $PM_{2.5}$ means recorded by SIMA are shown in Figure 10. $PM_{2.5}$ from MERRA-2 was calculated using Equation (2) following Buchard et al. (2016) [94], who multiplied the sulfate concentration by a factor of 1.375 because SO_4 is assumed to be primarily present in the form of neutralized ammonium sulfate ($(NH_4)_2SO_4$). OC is multiplied by a factor of 1.4 to estimate particulate organic matter (POM) [95]. This factor varies both spatially and temporally with values between 1.2 and 2.6 [96].

$$PM_{2.5} = [Dust_{2.5}] + [SS_{2.5}] + [BC] + 1.4 \times [OC] + 1.375 \times [SO_4] \quad (2)$$

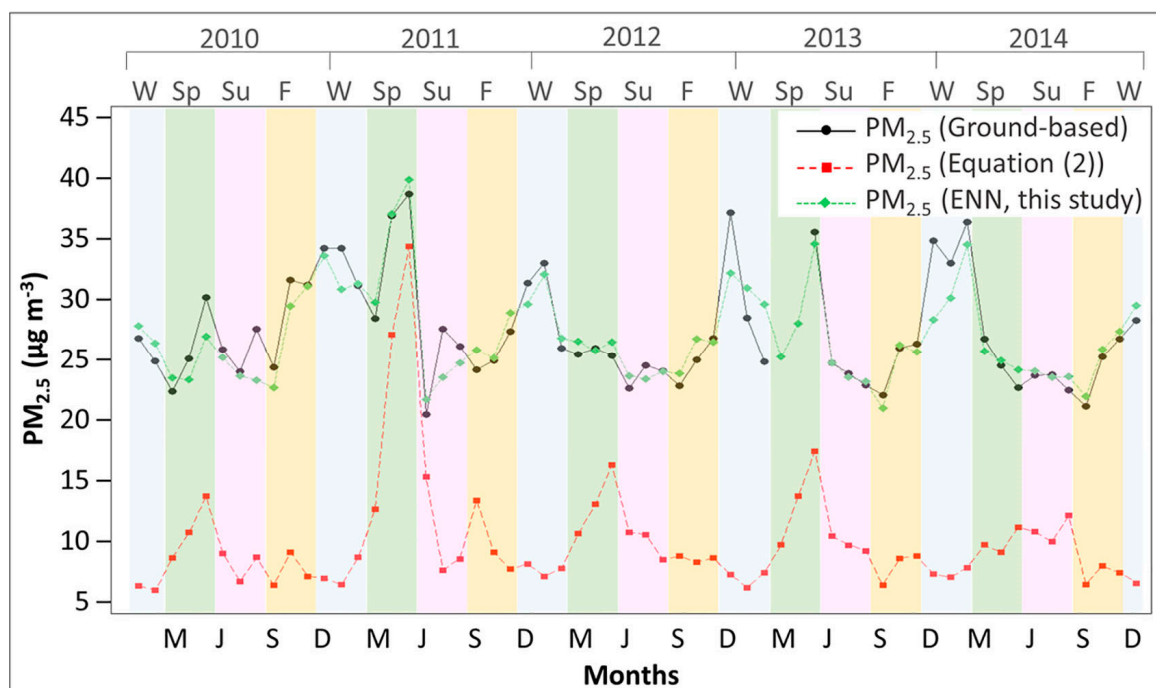


Figure 10. Comparisons of the monthly $PM_{2.5}$ means ($\mu\text{g m}^{-3}$) estimated by the NN developed in this study, MERRA-2 derived data, and SIMA data. Seasons: W: Winter, Sp: Spring, Su: Summer, F: Fall. Months: M: March; J: June, S: September, D: December.

PM_{2.5} concentrations were estimated using Equation (2), which included only PM_{2.5} components, were on average three times lower than those registered by SIMA. The differences between the observations and estimations were smaller in the spring and summer (by an average of 2.1 and 2.4 times, respectively) than in winter and fall (by an average of 4 and 3 times, respectively). Buchard et al. (2016) [94] evaluated MERRAero data (i.e., a version of aerosol products previously available before the release of MERRA-2 aerosol data) in the United States and found that the use of Equation (2) yielded closer-to-observation PM_{2.5} estimations during the summer, while larger discrepancies were observed during the winter. In this research, the PM_{2.5} estimations obtained by Equation (2) represented the peak of high concentrations observed in spring 2011, coincident with one of the worst years of drought in the northeastern region, according to the North American Drought Monitor of the NOAA. In comparing MERRA-2 reconstructed PM_{2.5} with ground observations one has to acknowledge that the former represents the average over a large volume, while the latter is representative of a spatial coverage of a few kilometers. Nonetheless it is valuable to compare these values as similarities and biases can be identified.

The MMA and the eastern part of the regional domain -particularly, the northeastern grid cells over Texas- showed high PM_{2.5} concentrations in summer and fall. The model's PM_{2.5} estimations were evaluated for two blind sites in order to analyze the ability of the ENN to capture the atmospheric dynamics in the lower Río Grande Valley. Monthly average PM_{2.5} concentrations at two monitoring sites located in Laredo, Texas (Lat 27.599°, Lon -99.533°) and McAllen, Texas (Lat 26.226° Lon -98.291°) were compared to ENN PM_{2.5} estimations in the grid cells where the Laredo (Lat 27.5°, Lon -100°, Lat 28.0°, Lon -99.375°) and McAllen (Lat 26°, Lon -98.750°, Lat 26.5°, Lon -98.125°) sites are located (Figure 2).

The correlations between the ground-based monthly averaged PM_{2.5} and the ENN PM_{2.5} estimations (Figure 11) at the blind sites were statistically significant (p -value < 0.01), with $R = 0.83$ and $RMSE = 7.63 \mu\text{g m}^{-3}$ for the Laredo site and $R = 0.73$ and $RMSE = 6.46 \mu\text{g m}^{-3}$ for McAllen. In addition, estimations of PM_{2.5} using Equation (2) over the blind sites and over MMA were performed and correlated with ground-based data. The statistical metrics obtained using Equation (2) were $R = 0.92$ and $RMSE = 3.66 \mu\text{g m}^{-3}$ at Laredo, $R = 0.82$ at and $RMSE = 5.11 \mu\text{g m}^{-3}$ at McAllen, and $R = 0.54$ and $RMSE = 17.07 \mu\text{g m}^{-3}$ at MMA. These correlation coefficients were found to be larger than expected, considering that PM_{2.5} values reported at the monitoring sites were on-point measurements, whereas the estimations represented the average of a grid cell. The $RMSE$ in the blind sites might indicate the potential issue of overestimation because the ENN model was trained and calibrated using only ground measurements from the MMA. The low R and high $RMSE$ values obtained using Equation (2) over the MMA indicated that using only PM_{2.5} components from MERRA-2 in a simple model is not enough to represent PM_{2.5} concentrations over the area.

The PM_{2.5} concentrations estimated by the ENN developed in this study showed the same temporal behavior as SIMA ground observations. These findings reinforce the usefulness of the methodology developed here. While the ENN was able to capture PM_{2.5} concentrations observed at the Laredo and McAllen sites with moderate accuracy, research is needed to improve the performance of the NNs to estimate the PM_{2.5} distribution in the entire region.

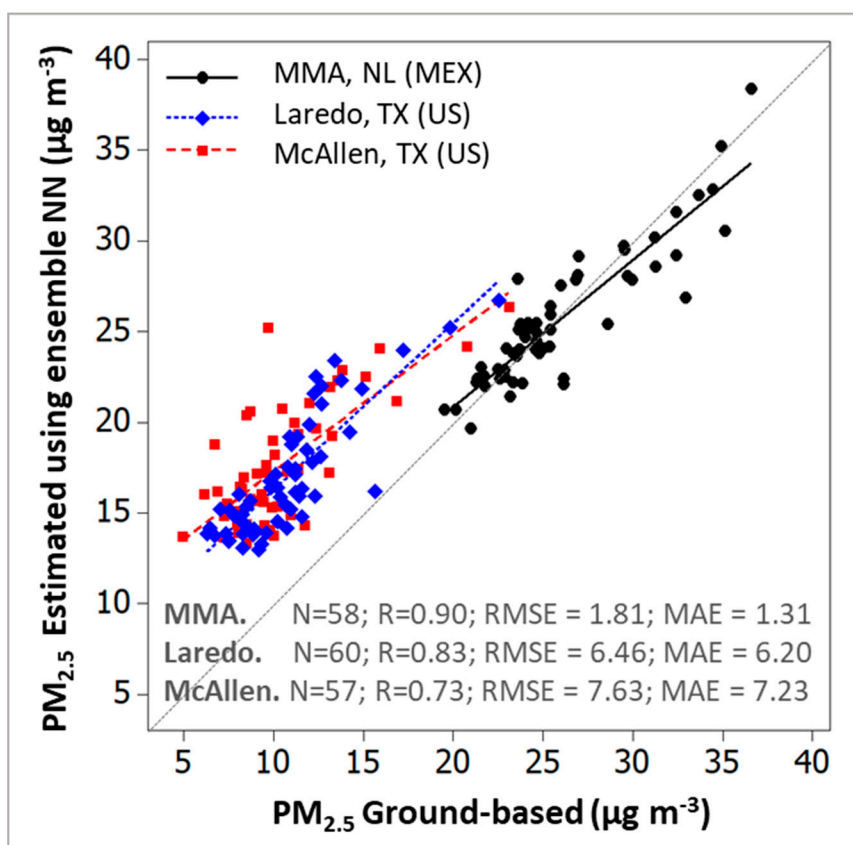


Figure 11. Comparison of the statistical performance obtained using the ENN to estimate monthly $PM_{2.5}$ means over the MMA, Laredo, and McAllen sites from January 2010 to December 2014.

5. Conclusions

The ability of MERRA-2 products to represent ground-based $PM_{2.5}$ measurements in the MMA was evaluated. Seasonal differences between MERRA2-AOD and ground-based $PM_{2.5}$ concentrations were observed. MERRA-2 meteorological products also yielded relatively well-represented monthly averaged ground-based temperatures and relative humidity but the wind components from MERRA-2 were not able to represent the predominant wind pattern (east-to-west direction) or the wind speeds observed in the MMA. Despite the dissimilarity in spatial and temporal resolutions, temporal patterns from MERRA-2 OC, BC, dust, and SS were consistent with the ground-based trends observed in previous studies carried out in the MMA. However, some variations in sulfate trends were found in summer compared with the rest of the year (MERRA-2 reported its lowest values in summer in contrast to ground-based studies that reported large sulfate concentrations in summer). Further research is recommended to understand the dilution effect and the relationship between air pollutants and urban morphology in the MMA.

The training fittings and cross-validation differences indicated that the model was robust and not over-fitted. The measure of bias showed seasonal dependence (the best performance was in spring; the worst was in winter) as in other regions of the world. Over the entire domain, high concentration levels were observed in spring, which was probably due to biomass burning; however, further research is recommended. Moderate to low concentrations emerged in fall and summer, respectively. The ENN was also able to capture the $PM_{2.5}$ concentration trends at the Laredo and McAllen sites in Texas. However, because the ENN model was trained and calibrated using only ground measurements from the MMA, the inclusion of all available ground data (e.g., Texan sites) is recommended to avoid overestimation and to enhance the calibration process and enable a better description of regional atmospheric dynamics.

The global coverage provided by the reanalysis datasets used in the methodology presented here could be easily replicated and used in the assessment of local and regional air quality applications, especially in regions where none or few PM_{2.5} ground-based stations are located. This application could provide a better understanding of the regional PM_{2.5} distribution and help improve current control strategies aimed at reducing PM_{2.5} pollution in NEM. It is suggested that in another stage of the research, new monitoring campaigns be carried out over the MMA and other sites within the NEM to further validate and compare the results with satellite data (i.e., MODIS and MERRA-2) and to segregate regional databases by season to improve the analysis of seasonal dynamics at the regional scale.

Author Contributions: Conceptualization, P.G., D.F.L.-G. and A.M.; Data curation, J.M.C.; Formal analysis, J.M.C., P.G., D.F.L.-G., A.Y.V. and F.D.Y.; Funding acquisition, A.M.; Investigation, J.M.C., A.Y.V. and F.D.Y.; Methodology, P.G., D.F.L.-G. and A.M.; Project administration, A.M.; Software, J.M.C.; Supervision, P.G., D.F.L.-G. and A.M.; Validation, P.G. and A.M.; Visualization, J.M.C. and F.D.Y.; Writing—original draft, J.M.C., A.Y.V. and F.D.Y.; Writing—review & editing, P.G., D.F.L.-G. and A.M. All authors have read and agreed to the published version of the manuscript.

Acknowledgments: This research was supported by Tecnológico de Monterrey, CONACYT (Grant Agreement PN 2014/247079), COLCIENCIAS, and USRA. Their support is gratefully acknowledged. Data provision and production were essential to the project. The surface data were provided by SIMA, and the MERRA-2 products were developed by the NASA-GMAO team.

Conflicts of Interest: The authors declare no conflict of interest.

References

- Cheng, Z.; Luo, L.; Wang, S.; Wang, Y.; Sharma, S.; Shimadera, H.; Wang, X.; Bressi, M.; Miranda, R.; Jiang, J.; et al. Status and characteristics of ambient PM_{2.5} pollution in global megacities. *Environ. Int.* **2016**, *89*, 89–90. [[CrossRef](#)] [[PubMed](#)]
- Fu, P.; Guo, X.; Cheung, F.M.H.; Yung, K.K.L. The association between PM_{2.5} exposure and neurological disorders: A systematic review and meta-analysis. *Sci. Total Environ.* **2019**, *655*, 1240–1248. [[CrossRef](#)]
- Gutiérrez-Avila, I.; Rojas-Bracho, L.; Riojas-Rodríguez, H.; Kloog, I.; Just, A.C.; Rothenberg, S.J. Cardiovascular and cerebrovascular mortality associated with acute exposure to PM_{2.5} in Mexico City. *Stroke* **2018**, *49*, 1734–1736. [[CrossRef](#)] [[PubMed](#)]
- Fajersztajn, L.; Saldiva, P.; Pereira, L.A.A.; Leite, V.F.; Buehler, A.M. Short-term effects of fine particulate matter pollution on daily health events in Latin America: A systematic review and meta-analysis. *Int. J. Public Health* **2017**, *62*, 729–738. [[CrossRef](#)] [[PubMed](#)]
- Yang, S.; Lee, S.-P.; Park, J.-B.; Lee, H.; Kang, S.-H.; Lee, S.-E.; Kim, J.B.; Choi, S.-Y.; Kim, Y.-J.; Chang, H.-J. PM_{2.5} concentration in the ambient air is a risk factor for the development of high-risk coronary plaques. *Eur. Heart J. Cardiovasc. Imaging* **2019**, *20*, 1355–1364. [[CrossRef](#)]
- Gao, M.; Cao, J.; Seto, E. A distributed network of low-cost continuous reading sensors to measure spatiotemporal variations of PM_{2.5} in Xi'an, China. *Environ. Pollut.* **2015**, *199*, 56–65. [[CrossRef](#)] [[PubMed](#)]
- Song, Z.; Fu, D.; Zhang, X.; Wu, Y.; Xia, X.; He, J. Diurnal and seasonal variability of PM_{2.5} and AOD in North China plain: Comparison of MERRA-2 products and ground measurements. *Atmos. Environ.* **2018**, *191*, 70–78. [[CrossRef](#)]
- Idrees, Z.; Zheng, L. Low cost air pollution monitoring systems: A review of protocols and enabling technologies. *J. Ind. Inf. Integr.* **2020**, *17*, 100123. [[CrossRef](#)]
- Riojas-Rodríguez, H.; Soares da Silva, A.; Texcalac Sangrador, J.L.; Moreno-Banda, G. Air pollution management and control in Latin America and the Caribbean: Implications for climate change. *Rev. Panam. De Salud Pública* **2016**, *40*, 150–159.
- PurpleAir. PurpleAir Map. Available online: <https://www.purpleair.com/map?opt=1/mAQI/a10/cC0#11/25.6414/-100.2937> (accessed on 16 March 2020).
- Gupta, P.; Doraiswamy, P.; Levy, R.; Pikelnaya, O.; Maibach, J.; Feenstra, B.; Polidori, A.; Kiros, F.; Mills, K.C. Impact of California fires on local and regional air quality: The role of a low-cost sensor network and satellite observations. *GeoHealth* **2018**, *2*, 172–181. [[CrossRef](#)]

12. Rogulski, M. Using low-cost PM monitors to detect local changes of air quality. *Pol. J. Environ. Stud.* **2018**, *27*. [[CrossRef](#)]
13. Chu, D.A.; Kaufman, Y.J.; Zibordi, G.; Chern, J.D.; Mao, J.; Li, C.; Holben, B.N. Global monitoring of air pollution over land from the earth observing system-terra moderate resolution imaging spectroradiometer (MODIS). *J. Geophys. Res. D Atmos.* **2003**, *108*, 1–18. [[CrossRef](#)]
14. van Donkelaar, A.; Martin, R.V.; Park, R.J. Estimating ground-level PM_{2.5} using aerosol optical depth determined from satellite remote sensing. *J. Geophys. Res. Atmos.* **2006**, *111*, 1–10. [[CrossRef](#)]
15. Levy, R.C.; Mattoo, S.; Munchak, L.A.; Remer, L.A.; Sayer, A.M.; Patadia, F.; Hsu, N.C. The collection 6 MODIS aerosol products over land and ocean. *Atmos. Meas. Tech.* **2013**, *6*, 2989–3034. [[CrossRef](#)]
16. Shin, S.-K.; Tesche, M.; Müller, D.; Noh, Y. Technical note: Absorption aerosol optical depth components from AERONET observations of mixed dust plumes. *Atmos. Meas. Tech.* **2019**, *12*, 607–618. [[CrossRef](#)]
17. Randles, C.A.; da Silva, A.M.; Buchard, V.; Colarco, P.R.; Darmenov, A.; Govindaraju, R.; Smirnov, A.; Holben, B.; Ferrare, R.; Hair, J.; et al. The MERRA-2 aerosol reanalysis, 1980 onward. Part I: System description and data assimilation evaluation. *J. Clim.* **2017**, *30*, 6823–6850. [[CrossRef](#)]
18. Provençal, S.; Kishcha, P.; da Silva, A.M.; Elhacham, E.; Alpert, P. AOD distributions and trends of major aerosol species over a selection of the world's most populated cities based on the 1st version of NASA's MERRA aerosol reanalysis. *Urban Clim.* **2017**, *20*, 168–191. [[CrossRef](#)]
19. Qin, W.; Zhang, Y.; Chen, J.; Yu, Q.; Cheng, S.; Li, W.; Liu, X.; Tian, H. Variation, sources and historical trend of black carbon in Beijing, China based on ground observation and MERRA-2 reanalysis data. *Environ. Pollut.* **2019**, *245*, 853–863. [[CrossRef](#)]
20. Xu, X.; Yang, X.; Zhu, B.; Tang, Z.; Wu, H.; Xie, L. Characteristics of MERRA-2 black carbon variation in east China during 2000–2016. *Atmos. Environ.* **2020**, *222*, 117140. [[CrossRef](#)]
21. Sitnov, S.A.; Mokhov, I.I.; Likhosherstova, A.A. Exploring large-scale black-carbon air pollution over Northern Eurasia in summer 2016 using MERRA-2 reanalysis data. *Atmos. Res.* **2020**, *235*, 104763. [[CrossRef](#)]
22. Mukkavilli, S.K.; Prasad, A.A.; Taylor, R.A.; Huang, J.; Mitchell, R.M.; Troccoli, A.; Kay, M.J. Assessment of atmospheric aerosols from two reanalysis products over Australia. *Atmos. Res.* **2019**, *215*, 149–164. [[CrossRef](#)]
23. García-Franco, J.L. Air quality in Mexico City during the fuel shortage of January 2019. *Atmos. Environ.* **2020**, *222*. [[CrossRef](#)]
24. Gardner, M.W.; Dorling, S.R. Artificial neural networks (the multilayer perceptron)—A review of applications in the atmospheric sciences. *Atmos. Environ.* **1998**, *32*, 2627–2636. [[CrossRef](#)]
25. Karimian, H.; Li, Q.; Wu, C.; Qi, Y.; Mo, Y.; Chen, G.; Zhang, X.; Sachdeva, S. Evaluation of different machine learning approaches to forecasting PM_{2.5} mass concentrations. *Aerosol Air Qual. Res.* **2019**, *19*, 1400–1410. [[CrossRef](#)]
26. Sadorsky, P. Modeling and forecasting petroleum futures volatility. *Energy Econ.* **2006**, *28*, 467–488. [[CrossRef](#)]
27. Bai, Y.; Li, Y.; Wang, X.; Xie, J.; Li, C. Air pollutants concentrations forecasting using back propagation neural network based on wavelet decomposition with meteorological conditions. *Atmos. Pollut. Res.* **2016**, *7*, 557–566. [[CrossRef](#)]
28. Chen, L.; Pai, T.Y. Comparisons of GM (1,1), and BPNN for predicting hourly particulate matter in Dali area of Taichung city, Taiwan. *Atmos. Pollut. Res.* **2015**, *6*, 572–580. [[CrossRef](#)]
29. Durão, R.M.; Mendes, M.T.; João Pereira, M. Forecasting O₃ levels in industrial area surroundings up to 24 h in advance, combining classification trees and MLP models. *Atmos. Pollut. Res.* **2016**, *7*, 961–970. [[CrossRef](#)]
30. Wang, D.; Wei-Zhen, L. Forecasting of ozone level in time series using MLP model with a novel hybrid training algorithm. *Atmos. Environ.* **2006**, *40*, 913–924. [[CrossRef](#)]
31. Iliyas, S.A.; Elshafei, M.; Habib, M.A.; Adeniran, A.A. RBF neural network inferential sensor for process emission monitoring. *Control Eng. Pract.* **2013**, *21*, 962–970. [[CrossRef](#)]
32. Lu, W.Z.; Wang, W.J.; Wang, X.K.; Yan, S.H.; Lam, J.C. Potential assessment of a neural network model with PCA/RBF approach for forecasting pollutant trends in Mong Kok urban air, Hong Kong. *Environ. Res.* **2004**, *96*, 79–87. [[CrossRef](#)] [[PubMed](#)]
33. Maleki, H.; Sorooshian, A.; Goudarzi, G.; Baboli, Z.; Tahmasebi Birgani, Y.; Rahmati, M. Air pollution prediction by using an artificial neural network model. *Clean Technol. Environ. Policy* **2019**, *21*, 1341–1352. [[CrossRef](#)]
34. Prasad, K.; Gorai, A.K.; Goyal, P. Development of ANFIS models for air quality forecasting and input optimization for reducing the computational cost and time. *Atmos. Environ.* **2016**, *128*, 246–262. [[CrossRef](#)]

35. Taheri Shahraiyni, H.; Sodoudi, S.; Kerschbaumer, A.; Cubasch, U. A new structure identification scheme for ANFIS and its application for the simulation of virtual air pollution monitoring stations in urban areas. *Eng. Appl. Artif. Intell.* **2015**, *41*, 175–182. [CrossRef]
36. Cabaneros, S.M.; Calautit, J.K.; Hughes, B.R. A review of artificial neural network models for ambient air pollution prediction. *Environ. Model. Softw.* **2019**, *119*, 285–304. [CrossRef]
37. Liu, Y. New directions: Satellite driven PM_{2.5} exposure models to support targeted particle pollution health effects research. *Atmos. Environ.* **2013**, *68*, 52–53. [CrossRef]
38. Secretaría de Desarrollo Agrario, Territorial y Urbano, Consejo Nacional de Población and Instituto Nacional de Estadística y Geografía. In *Delimitación de las Zonas Metropolitanas de México 2015*; Secretaría de Gobernación: Mexico City, Mexico, 2018.
39. González-Santiago, O.; Badillo-Castañeda, C.T.; Kahl, J.D.W.; Ramírez-Lara, E.; Balderas-Renteria, I. Temporal analysis of PM₁₀ in metropolitan Monterrey, México. *J. Air Waste Manag. Assoc.* **2011**, *61*, 573–579. [CrossRef] [PubMed]
40. Menchaca-Torre, H.L.; Mercado-Hernández, R.; Rodríguez-Rodríguez, J.; Mendoza-Domínguez, A. Diurnal and seasonal variations of carbonyls and their effect on ozone concentrations in the atmosphere of Monterrey, Mexico. *J. Air Waste Manag. Assoc.* **2015**, *65*, 500–510. [CrossRef]
41. Mancilla, Y.; Mendoza, A. A tunnel study to characterize PM_{2.5} emissions from gasoline-powered vehicles in Monterrey, Mexico. *Atmos. Environ.* **2012**, *59*, 449–460. [CrossRef]
42. Secretaría de Medio Ambiente y Recursos Naturales. Inventario Nacional de Emisiones de Contaminantes Criterio (INEM 2016). Available online: <https://www.gob.mx/semarnat/documentos/documentos-del-inventario-nacional-de-emisiones> (accessed on 22 February 2020).
43. Mancilla, Y.; Herckes, P.; Fraser, M.P.; Mendoza, A. Secondary organic aerosol contributions to PM_{2.5} in Monterrey, Mexico: Temporal and seasonal variation. *Atmos. Res.* **2015**, *153*, 348–359. [CrossRef]
44. Martínez, M.A.; Caballero, P.; Carrillo, O.; Mendoza, A.; Mejía, G.M. Chemical characterization and factor analysis of PM_{2.5} in two sites of Monterrey, Mexico. *J. Air Waste Manag. Assoc.* **2012**, *62*, 817–827. [CrossRef] [PubMed]
45. Mancilla, Y.; Mendoza, A.; Fraser, M.P.; Herckes, P. Organic composition and source apportionment of fine aerosol at Monterrey, Mexico, based on organic markers. *Atmos. Chem. Phys.* **2016**, *16*, 953–970. [CrossRef]
46. Medina, G. Desarrollo de perfiles de emisión de la fracción orgánica del PM_{2.5} en el Área Metropolitana de Monterrey. Master's Thesis, Instituto Tecnológico y de Estudios Superiores de Monterrey, Monterrey, Mexico, December 2015.
47. Trejo-González, A.G.; Riojas-Rodríguez, H.; Texcalac-Sangrador, J.L.; Guerrero-López, C.M.; Cervantes-Martínez, K.; Hurtado-Díaz, M.; de la Sierra-de la Vega, L.A.; Zuñiga-Bello, P.E. Quantifying health impacts and economic costs of PM_{2.5} exposure in Mexican cities of the national urban system. *Int. J. Public Health* **2019**, *64*, 561–572. [CrossRef] [PubMed]
48. Mancilla, Y.; Hernández Paniagua, I.Y.; Mendoza, A. Spatial differences in ambient coarse and fine particles in the Monterrey metropolitan area, Mexico: Implications for source contribution. *J. Air Waste Manag. Assoc.* **2019**, *69*, 548–564. [CrossRef]
49. Blanco-Jiménez, S.; Altúzar, F.; Jiménez, B.; Aguilar, G.; Pablo, M.; Benítez, M.A. *Evaluación de las Partículas Suspendidas PM_{2.5} en el Área Metropolitana de Monterrey*; Instituto Nacional de Ecología y Cambio Climático (INECC): Mexico City, Mexico, 2015.
50. Secretaría de Medio Ambiente y Recursos Naturales. Norma Oficial Mexicana NOM-035-SEMARNAT-1993. In *Métodos de Medición para Determinar la Concentración de Partículas Suspendidas Totales en el Aire Ambiente y los Procedimientos para la Calibración de los Equipos de Medición*; Diario Oficial de la Federación: Mexico City, Mexico, 1993.
51. Secretaría de Medio Ambiente y Recursos Naturales Norma Oficial Mexicana NOM-156-SEMARNAT-2012, *Establecimiento y Operación de Sistemas de Monitoreo de la Calidad del Aire*; Diario Oficial de la Federación: Mexico City, Mexico, 2012.
52. Rienecker, M.M.; Suarez, M.J.; Gelaro, R.; Todling, R.; Bacmeister, J.; Liu, E.; Bosilovich, M.G.; Schubert, S.D.; Takacs, L.; Kim, G.K.; et al. MERRA: NASA's modern-era retrospective analysis for research and applications. *J. Clim.* **2011**, *24*, 3624–3648. [CrossRef]

53. Buchard, V.; Randles, C.A.; da Silva, A.M.; Darmenov, A.; Colarco, P.R.; Govindaraju, R.; Ferrare, R.; Hair, J.; Beyersdorf, A.J.; Ziemba, L.D.; et al. The MERRA-2 aerosol reanalysis, 1980 onward. Part II: Evaluation and case studies. *J. Clim.* **2017**, *30*, 6851–6872. [[CrossRef](#)]
54. Mahesh, B.; Rama, B.V.; Spandana, B.; Sarma, M.S.S.R.K.N.; Niranjan, K.; Sreekanth, V. Evaluation of MERRAero PM_{2.5} over Indian cities. *Adv. Space Res.* **2019**, *64*, 328–334. [[CrossRef](#)]
55. Gelaro, R.; McCarty, W.; Suárez, M.J.; Todling, R.; Molod, A.; Takacs, L.; Randles, C.A.; Darmenov, A.; Bosilovich, M.G.; Reichle, R.; et al. The modern-era retrospective analysis for research and applications, version 2 (MERRA-2). *J. Clim.* **2017**, *30*, 5419–5454. [[CrossRef](#)]
56. Global Modeling and Assimilation Office (GMAO). M2IMNPASM—MERRA-2 instM_3d_asm_Np: 3d, Monthly Mean, Time-Averaged, Pressure-Level, Assimilated Meteorological Fields V5.12.4; Goddard Earth Sciences Data and Information Services Center (GES DISC): Greenbelt, MD, USA, 2015. [[CrossRef](#)]
57. Global Modeling and Assimilation Office (GMAO). M2TMNXFLX—MERRA-2 tavgM_2d_flux_Nx: 2d, Monthly Mean, Time-Averaged, Single-Level, Assimilation, Surface Flux Diagnostics V5.12.4; Goddard Earth Sciences Data and Information Services Center (GES DISC): Greenbelt, MD, USA, 2015. [[CrossRef](#)]
58. Global Modeling and Assimilation Office (GMAO). M2TMNXAER—MERRA-2 tavgM_2d_aer_Nx: 2d, Monthly Mean, Time-Averaged, Single-Level, Assimilation, Aerosol Diagnostics V5.12.4; Goddard Earth Sciences Data and Information Services Center (GES DISC): Greenbelt, MD, USA, 2015. [[CrossRef](#)]
59. Secretaría de Salud. Norma Oficial Mexicana NOM-025-SSA1-2014. Salud Ambiental. Valores Límite Permisibles para la Concentración de Partículas Suspensas PM₁₀ y PM_{2.5} en el Aire Ambiente y Criterios para su Evaluación; Diario Oficial de la Federación: Mexico City, Mexico, 2014.
60. Chu, Y.; Liu, Y.; Li, X.; Liu, Z.; Lu, H.; Lu, Y.; Mao, Z.; Chen, X.; Li, N.; Ren, M.; et al. A review on predicting ground PM_{2.5} concentration using satellite aerosol optical depth. *Atmosphere* **2016**, *7*, 129. [[CrossRef](#)]
61. Hoff, R.M.; Christopher, S.A. Remote sensing of particulate pollution from space: Have we reached the promised land? *J. Air Waste Manag. Assoc.* **2009**, *59*, 645–675. [[CrossRef](#)]
62. Gupta, P.; Christopher, S.A. Particulate matter air quality assessment using integrated surface, satellite, and meteorological products: Multiple regression approach. *J. Geophys. Res.* **2009**, *114*, D14205. [[CrossRef](#)]
63. Shepherd, A.J. *Second-Order Methods for Neural Networks: Fast and Reliable Training Methods for Multi-Layer Perceptrons*; Springer: London, UK, 1997; p. 145. ISBN 978-1-4471-0953-2.
64. Prechelt, L. Automatic early stopping using cross validation: Quantifying the criteria. *Neural Netw.* **1998**, *11*, 761–767. [[CrossRef](#)]
65. Malhotra, R. *Empirical Research in Software Engineering: Concepts, Analysis, and Applications*; CRC Press: London, UK, 2016; ISBN 978-1-4987-1973-5.
66. Koul, A.; Becchio, C.; Cavallo, A. Cross-validation approaches for replicability in psychology. *Front. Psychol.* **2018**, *9*. [[CrossRef](#)] [[PubMed](#)]
67. Chen, S.H.; Jakeman, A.J.; Norton, J.P. Artificial intelligence techniques: An introduction to their use for modelling environmental systems. *Math. Comput. Simul.* **2008**, *78*, 379–400. [[CrossRef](#)]
68. Jiang, D.; Zhang, Y.; Hu, X.; Zeng, Y.; Tan, J.; Shao, D. Progress in developing an ANN model for air pollution index forecast. *Atmos. Environ.* **2004**, *38*, 7055–7064. [[CrossRef](#)]
69. Sarle, W.S. Stopped training and other remedies for overfitting. In Proceedings of the 27th Symposium on the Interface of Computing Science and Statistics, Pittsburgh, PA, USA, 21–24 June 1995; pp. 352–360.
70. Mao, X.; Shen, T.; Feng, X. Prediction of hourly ground-level PM_{2.5} concentrations 3 days in advance using neural networks with satellite data in eastern China. *Atmos. Pollut. Res.* **2017**. [[CrossRef](#)]
71. Shao, Y.; Taff, G.N.; Walsh, S.J. Comparison of early stopping criteria for neural-network-based subpixel classification. *IEEE Geosci. Remote Sens. Lett.* **2011**, *8*, 113–117. [[CrossRef](#)]
72. NOAA. National Oceanic and Atmospheric Administration Aerosol Optical Depth. Available online: <http://www.esrl.noaa.gov/gmd/grad/surfrad/aod/> (accessed on 20 February 2020).
73. Guo, Y.; Tang, Q.; Gong, D.Y.; Zhang, Z. Estimating ground-level PM_{2.5} concentrations in Beijing using a satellite-based geographically and temporally weighted regression model. *Remote Sens. Environ.* **2017**, *198*, 140–149. [[CrossRef](#)]
74. Li, T.; Shen, H.; Zeng, C.; Yuan, Q.; Zhang, L. Point-surface fusion of station measurements and satellite observations for mapping PM_{2.5} distribution in China: Methods and assessment. *Atmos. Environ.* **2017**, *152*, 477–489. [[CrossRef](#)]

75. Liu, Y.; Franklin, M.; Kahn, R.; Koutrakis, P. Using aerosol optical thickness to predict ground-level PM_{2.5} concentrations in the St. Louis area: A comparison between MISR and MODIS. *Remote Sens. Environ.* **2007**, *107*, 33–44. [[CrossRef](#)]
76. Ma, X.; Yu, F. Seasonal variability of aerosol vertical profiles over east US and west Europe: GEOS-Chem/APM simulation and comparison with CALIPSO observations. *Atmos. Res.* **2014**, *140–141*, 28–37. [[CrossRef](#)]
77. Song, W.; Jia, H.; Huang, J.; Zhang, Y. A satellite-based geographically weighted regression model for regional PM_{2.5} estimation over the Pearl River Delta region in China. *Remote Sens. Environ.* **2014**, *154*, 1–7. [[CrossRef](#)]
78. You, W.; Zang, Z.; Zhang, L.; Li, Y.; Pan, X.; Wang, W. National-scale estimates of ground-level PM_{2.5} concentration in China using geographically weighted regression based on 3 km resolution MODIS AOD. *Remote Sens.* **2016**, *8*, 184. [[CrossRef](#)]
79. Kong, L.; Xin, J.; Liu, Z.; Zhang, K.; Zhang, W.; Wang, Y. The PM_{2.5} threshold for aerosol extinction in the Beijing megacity. *Atmos. Environ.* **2017**, *167*. [[CrossRef](#)]
80. Carrillo-Torres, E.R.; Hernández-Paniagua, I.Y.; Mendoza, A. Use of combined observational- and model-derived photochemical indicators to assess the O₃-NO_x-VOC system sensitivity in urban areas. *Atmosphere* **2017**, *8*, 22. [[CrossRef](#)]
81. Martínez-Cinco, M.; Santos-Guzmán, J.; Mejía-Velázquez, G. Source apportionment of PM_{2.5} for supporting control strategies in the Monterrey Metropolitan Area, Mexico. *J. Air Waste Manag. Assoc.* **2016**, *66*, 631–642. [[CrossRef](#)]
82. González, L.T.; Longoria-Rodríguez, F.E.; Sánchez-Domínguez, M.; Leyva-Porras, C.; Acuña-Askar, K.; Kharissov, B.I.; Arizpe-Zapata, A.; Alfaro-Barbosa, J.M. Seasonal variation and chemical composition of particulate matter: A study by XPS, ICP-AES and sequential microanalysis using Raman with SEM/EDS. *J. Environ. Sci.* **2018**, *74*, 32–49. [[CrossRef](#)]
83. Wang, F.; Zhang, Z.; Chambers, S.; Tian, X.; Zhu, R.; Mei, M.; Huang, Z.; Allegrini, I. Quantifying influences of nocturnal mixing on air quality using atmospheric radon measurement-case study in Jinhua city, China. *Aerosol Air Qual. Res.* **2020**. [[CrossRef](#)]
84. Fernando, H.J.S.; Lee, S.M.; Anderson, J.; Princevac, M.; Pardyjak, E.; Grossman-Clarke, S. Urban fluid mechanics: Air circulation and contaminant dispersion in cities. *Environ. Fluid Mech.* **2001**, *1*, 107–164. [[CrossRef](#)]
85. Peralta, O.; Ortíz-Alvarez, A.; Basaldud, R.; Santiago, N.; Alvarez-Ospina, H.; de la Cruz, K.; Barrera, V.; de la Luz Espinosa, M.; Saavedra, I.; Castro, T.; et al. Atmospheric black carbon concentrations in Mexico. *Atmos. Res.* **2019**, *230*, 104626. [[CrossRef](#)]
86. Hernández Paniagua, I.Y.; Clemitshaw, K.C.; Mendoza, A. Observed trends in ground-level O₃ in Monterrey, Mexico, during 1993–2014: Comparison with Mexico City and Guadalajara. *Atmos. Chem. Phys.* **2017**, *17*, 9163–9185. [[CrossRef](#)]
87. Cao, J.J.; Wu, F.; Chow, J.C.; Lee, S.C.; Li, Y.; Chen, S.W.; An, Z.S.; Fung, K.K.; Watson, J.G.; Zhu, C.S.; et al. Characterization and source apportionment of atmospheric organic and elemental carbon during fall and winter of 2003 in Xi'an, China. *Atmos. Chem. Phys.* **2005**, *5*, 3127–3137. [[CrossRef](#)]
88. Cabada, J.C.; Pandis, S.N.; Subramanian, R.; Robinson, A.L.; Polidori, A.; Turpin, B. Estimating the secondary organic aerosol contribution to PM_{2.5} using the EC tracer method special issue of aerosol science and technology on findings from the fine particulate matter supersites program. *Aerosol Sci. Technol.* **2004**, *38*, 140–155. [[CrossRef](#)]
89. Su, T.; Li, J.; Li, C.; Lau, A.K.H.; Yang, D.; Shen, C. An intercomparison of AOD-converted PM_{2.5} concentrations using different approaches for estimating aerosol vertical distribution. *Atmos. Environ.* **2017**, *166*, 531–542. [[CrossRef](#)]
90. Alvarado, M.J.; McVey, A.E.; Hegarty, J.D.; Cross, E.S.; Hasenkopf, C.A.; Lynch, R.; Kennelly, E.J.; Onasch, T.B.; Awe, Y.; Sanchez-Triana, E.; et al. Evaluating the use of satellite observations to supplement ground-level air quality data in selected cities in low- and middle-income countries. *Atmos. Environ.* **2019**, *218*, 117016. [[CrossRef](#)]
91. He, L.; Lin, A.; Chen, X.; Zhou, H.; Zhou, Z.; He, P. Assessment of MERRA-2 Surface PM_{2.5} over the Yangtze River Basin: Ground-based verification, spatiotemporal distribution and meteorological dependence. *Remote Sens.* **2019**, *11*, 460. [[CrossRef](#)]
92. Wang, S.; Zhou, C.; Wang, Z.; Feng, K.; Hubacek, K. The characteristics and drivers of fine particulate matter (PM_{2.5}) distribution in China. *J. Clean. Prod.* **2017**, *142*, 1800–1809. [[CrossRef](#)]

93. Hu, H.; Hu, Z.; Zhong, K.; Xu, J.; Zhang, F.; Zhao, Y.; Wu, P. Satellite-based high-resolution mapping of ground-level PM_{2.5} concentrations over East China using a spatiotemporal regression kriging model. *Sci. Total Environ.* **2019**, *672*, 479–490. [[CrossRef](#)]
94. Buchard, V.; da Silva, A.M.; Randles, C.A.; Colarco, P.; Ferrare, R.; Hair, J.; Hostetler, C.; Tackett, J.; Winker, D. Evaluation of the surface PM_{2.5} in version 1 of the NASA MERRA aerosol reanalysis over the United States. *Atmos. Environ.* **2016**, *125*, 100–111. [[CrossRef](#)]
95. Malm, W.C.; Sisler, J.F.; Huffman, D.; Eldred, R.A.; Cahill, T.A. Spatial and seasonal trends in particle concentration and optical extinction in the United States. *J. Geophys. Res.* **1994**, *99*, 1347. [[CrossRef](#)]
96. Malm, W.C.; Schichtel, B.A.; Pitchford, M.L. Uncertainties in PM_{2.5} gravimetric and speciation measurements and what we can learn from them. *J. Air Waste Manag. Assoc.* **2011**, *61*, 1131–1149. [[CrossRef](#)] [[PubMed](#)]



© 2020 by the authors. Licensee MDPI, Basel, Switzerland. This article is an open access article distributed under the terms and conditions of the Creative Commons Attribution (CC BY) license (<http://creativecommons.org/licenses/by/4.0/>).